NeuroImage 202 (2019) 116005

Contents lists available at ScienceDirect

NeuroImage

journal homepage: www.elsevier.com/locate/neuroimage

Nuisance effects in inter-scan functional connectivity estimates before and after nuisance regression

Alican Nalci [a,b,*], Wenjing Luo [a], Thomas T. Liu [a,c,**]

[a] Center for Functional MRI, University of California San Diego, 9500 Gilman Drive MC 0677, La Jolla, CA, 92093, USA
[b] Department of Electrical and Computer Engineering, University of California San Diego, 9500 Gilman Drive, La Jolla, CA, 92093, USA
[c] Departments of Radiology, Psychiatry, and Bioengineering, University of California San Diego, 9500 Gilman Drive, La Jolla, CA, 92093, USA

ARTICLE INFO

Keywords:
functional connectivity
Nuisance regression
Global signal
Variability

ABSTRACT

In resting-state functional MRI, the correlation between blood-oxygenation-level-dependent (BOLD) signals across brain regions is used to estimate the functional connectivity (FC) of the brain. FC estimates are prone to the influence of nuisance factors including scanner-related artifacts and physiological modulations of the BOLD signal. Nuisance regression is widely performed to reduce the effect of nuisance factors on FC estimates on a per-scan basis. However, a dedicated analysis of nuisance effects on the variability of FC metrics across a collection of scans has been lacking. This work investigates the effects of nuisance factors on the variability of FC estimates across a collection of scans both before and after nuisance regression. Inter-scan variations in FC estimates are shown to be significantly correlated with the geometric norms of various nuisance terms, including head motion measurements, signals derived from white-matter and cerebrospinal regions, and the whole-brain global signal (GS) both before and after nuisance regression. In addition, it is shown that GS regression (GSR) can introduce GS norm-related fluctuations that are negatively correlated with inter-scan FC estimates. The empirical results are shown to be largely consistent with the predictions of a theoretical framework previously developed for the characterization of dynamic FC measures. This work shows that caution must be exercised when interpreting inter-scan FC measures across scans both before and after nuisance regression.

1. Introduction

Resting-state functional magnetic resonance imaging (fMRI) is a widely used method that aims to characterize the functional organization of the brain at rest (Smith et al., 2012; Fox and Raichle, 2007). The blood-oxygenation-level-dependent (BOLD) signal reflects metabolic changes in the brain that result from neuronal activity (Biswal et al., 1995; Hallquist et al., 2013). The correlation between BOLD signals across different brain regions is computed to estimate the functional connectivity (FC) of the brain (Raichle et al., 2001; Fox et al., 2005).

It is well-known that the BOLD signal is prone to the influence of various nuisance confounds including thermal noise, scanner drift, head motion, and physiological activity such as changes in respiration and heart rate (Bright and Murphy, 2015; Bright et al., 2017; Hallquist et al., 2013; Birn et al., 2008; Chang et al., 2009). If these confounds are not removed from the BOLD signal prior to analysis, they can lead to an increase in the number of false positives and negatives, causing erroneous interpretations of the fMRI results (Glasser et al., 2018).

Nuisance regression (NR) is widely performed to improve the spatial specificity of FC estimates on a per-scan basis. This involves projecting out a combination of nuisance measurements from the BOLD data prior to the computation of FC estimates. Nuisance measurements typically include but are not limited to head motion (HM) measurements, signals from the white-matter (WM) and cerebrospinal fluid (CSF) regions, cardiac and respiratory activity derived time courses, and the whole-brain global signal (GS) (Murphy et al., 2013; Liu, 2016; Liu et al., 2017).

Despite the fact that NR is adopted with the assumption that it removes nuisance confounds from the FC estimates, it has been previously shown that it can be quiet ineffective in reducing the effects of nuisance confounds (Bright and Murphy, 2015; Power et al., 2012; Nalci et al., 2019). For example, HM regression has been shown to be a largely ineffective approach for reducing HM confounds in FC estimates even after projecting out 12 motion regressors (Power et al., 2012; Satterthwaite et al., 2012; Van Dijk et al., 2012).

* Corresponding author. Center for Functional MRI, University of California San Diego, 9500 Gilman Drive MC 0677, La Jolla, CA, 92093, USA.
** Corresponding author. Center for Functional MRI, University of California San Diego, 9500 Gilman Drive MC 0677, La Jolla, CA, 92093, USA.
E-mail addresses: analci@ucsd.edu (A. Nalci), ttliu@ucsd.edu (T.T. Liu).

https://doi.org/10.1016/j.neuroimage.2019.07.018
Received 9 April 2019; Received in revised form 6 June 2019; Accepted 8 July 2019
Available online 20 July 2019

More recently, in Nalci et al. (2019), we demonstrated that *dynamic* FC (DFC) estimates were related (within a scan) to the norms of various nuisance regressors such as the HM, WM+CSF, GS, heart rate, and respiratory derived time courses. We found that NR was largely ineffective in removing nuisance effects from DFC estimates with significant relations between the nuisance norms and DFC estimates remaining even after NR. We presented a theoretical framework to explain the limited effectiveness of NR and showed that the effects of nuisance norms on the DFC estimates were significant even when the correlations between the raw nuisance and BOLD signals were relatively small.

The fundamental difference between DFC and FC studies is the temporal duration over which the FC estimates (correlations between BOLD signals) are computed. In DFC studies the temporal window is typically on the order of 30–60 s, whereas in *static* FC studies the duration is the whole scan duration, which is typically several minutes or longer (Hutchison et al., 2013; Preti et al., 2017). We will use the terms FC and static FC in an interchangeable fashion.

Although the effects of nuisance terms and efficacy of NR have been investigated on a per-scan basis (Liu et al., 2017), efforts to examine nuisance effects with regards to variations in FC estimates across scans have been rather limited. A better understanding of these effects is critical considering the increasing use of fMRI to examine the differences in FC measures between disease populations and healthy controls (Van Den Heuvel and Pol, 2010). Relevant studies include the investigation of FC metrics in Alzheimer's disease (Greicius et al., 2004; Yang et al., 2014; Wang et al., 2007), Parkinson's disease (Baudrexel et al., 2011), depression (Greicius et al., 2007), schizoprenia (Liu et al., 2008), dementia (Rombouts et al., 2009), and amyotrophic lateral sclerosis (ALS) (Mohammadi et al., 2009; Agosta et al., 2013).

In this work, we first investigate the effects of nuisance terms on the variability of FC estimates across different scans. Specifically, for each scan we compute the norms of the HM measurements, WM+CSF time courses, and the GS. We show the existence of significant correlations across scans between the FC estimates and each of the nuisance norms. In light of this finding, there exists the possibility that differences in static FC estimates may partly reflect variations in the relative strengths of nuisance effects, thereby complicating the interpretation of studies comparing FC estimates across subjects, groups, or conditions (Van Den Heuvel and Pol, 2010; Greicius et al., 2004; Wang et al., 2007; Baudrexel et al., 2011). Thus, it is important to determine if nuisance regression can significantly reduce the relationship between FC estimates and nuisance norms. We find nuisance regression using non-GS regressors to be largely ineffective in reducing the correlations between FC estimates and nuisance norms. We show that although GSR is partially effective in reducing the relation between GS norm and FC estimates, a considerable portion of the GS norm-related variance remains in the FC estimates, and strong GS norm-related fluctuations can be injected into the FC estimates.

Our work significantly extends the preliminary results regarding static FC estimates presented in Nalci et al. (2019). We provide a more extensive analysis of various nuisance effects on the FC estimates before and after NR. We generalize the theory developed in Nalci et al. (2019) to static FC measures and confirm the validity of the theoretical limitation of nuisance regression for correlation-based static FC estimates. We introduce *nuisance contamination maps*, which illustrate the spatial distribution and extent of correlations between nuisance norms and FC estimates across scans. We also provide a detailed analysis of the limited efficacy of GSR and show how GSR can introduce GS norm-related fluctuations into the FC estimates.

2. Methods

2.1. Data

We used a publicly available dataset originally analyzed by Fox et al. (2007). The data were acquired from 17 young adults using a 3T Siemens Allegra MRI scanner. Each subject underwent 4 BOLD echo-planar imaging (EPI) scans (32 slices, TR = 2.16 s, TE = 25 ms, 4 × 4 × 4 mm) each lasting 7 min (194 frames). The subjects were instructed to look at a cross-hair and asked to remain still and awake. High-resolution T1-weighted anatomical images were acquired for the purpose of anatomical registration (TR = 2.1 s, TE = 3.93 ms, flip angle = 7 deg, 1 × 1 × 1.25 mm).

Standard pre-processing steps were conducted with the AFNI software package (Cox, 1996). The initial 9 frames from each EPI run were discarded to minimize longitudinal relaxation effects. Images were then slice-time corrected and co-registered, and the 6 head motion parameter time series were retained. The images were converted to Talairach and Tournoux (TT) coordinates, resampled to 3 mm cubic voxels, and spatially smoothed using a 6 mm full-width-at-half-maximum isotropic Gaussian kernel. The 0^{th} and 1^{st} order Legendre polynomials (a constant term to model the temporal mean and a linear trend) were projected out from each voxel's time course. Each voxel time series was then converted into a percent change BOLD time series through division by the estimate of the temporal mean. This version of the data will be referred to as uncorrected data in this paper.

We used seed signals derived from the posterior cingulate cortex (PCC), intraparietal sulcus (IPS), frontal eye fields (FEF), medial prefrontal cortex (MPF), auditory (AUD), and motor (MOT) networks. These seed signals were obtained by averaging time series selected over spheres of radius 6 mm (2 voxels) centered about their corresponding TT coordinates (He and Liu, 2012). The sphere centers were obtained by converting the MNI coordinates from Van Dijk et al. (2010) to TT coordinates (Lacadie et al., 2008). For the PCC, IPS, FEF and MPF seeds we used the coordinates [0,-51,26], [32,-51,41], [24,-13,51], and [6,32,28], respectively. For the left MOT, and right MOT seeds we used the coordinates [-36,-22,52] and [37,-12,52], respectively. A combined MOT seed was obtained by using the left and right MOT coordinates to define two spheres and by merging the spheres. A combined AUD seed was obtained by using the left and right AUD coordinates [-41,-26,14] and [41,-26,14], respectively. Finally, for the WM and CSF nuisance signals we defined the sphere centers as [31,-28,32] and [-15,-28,21], respectively.

2.2. Inter-scan variations in FC estimates

To investigate the variations in FC estimates across scans, we computed the Pearson correlation between a seed signal and every other voxel in the brain for each scan. For the kth scan, we denote the zero mean percent change BOLD signals from a seed-voxel pair as $x_{1,k}$ and $x_{2,k}$ in vector notation. The FC estimate was obtained by computing $\mathrm{FC}_k = (x_{1,k}^T x_{2,k})/(|x_{1,k}||x_{2,k}|)$, where $|.|$ denotes the ℓ_2 norm. For each seed-voxel pair, we computed the FC estimates across all scans and concatenated them to form a vector of FC estimates: $\mathrm{FC}_{\mathrm{Vec}} = \{\mathrm{FC}_1, \mathrm{FC}_2, \ldots, \mathrm{FC}_k, \ldots, \mathrm{FC}_K\}$ where $K = 68$ is the total number of scans. This vector will be referred to as the inter-scan FC estimates or simply as FC estimates. We obtained a separate vector $\mathrm{FC}_{\mathrm{Vec}}$ for each seed voxel pair in the brain (i.e. for a single seed, we have N vectors where N is the number of voxels).

2.3. Nuisance regressions

To investigate the effects of nuisance regression on FC estimates, we performed 4 separate nuisance regressions on the uncorrected data. This was done prior to the computation of FC estimates. Nuisance regressions involved projecting out (1) 6 HM parameters, (2) 6 HM parameters combined with the signals from the WM and CSF regions, (3) the GS time course, and (4) HM, WM, CSF signals combined with the GS. The global signal (GS) was obtained as the average of all (percent) change BOLD time courses across the whole brain volume. For each nuisance regression, the vector of inter-scan FC estimates prior to nuisance regression will be referred to as "Pre FC" estimates and after regression as "Post FC" estimates.

2.4. Norm as a nuisance metric on FC estimates across scans

To measure the effect of nuisance terms on the FC estimates across scans we adopted the approach in Nalci et al. (2019). For GS regression, we first computed the ℓ_2 norm of the GS time course for each scan. Denoting the GS time course for a scan k with n_k, we computed the ℓ_2 norm as $|n_k| = \sqrt{\sum_{t=1}^{T} n_k^2(t)}$, where t indexes over time and T is the total number of time points. We then concatenated the GS norms across different scans to obtain a vector of GS norms as $|n|_{\text{Vec}} = \{|n_1|, |n_2|, \ldots, |n_k|, \ldots, |n_K|\}$.

For multiple nuisance regressions (e.g. HM+WM+CSF) we obtained a total norm of all the regressors involved by computing $|n_k| = \sqrt{\sum_{i=1}^{N_R} \sum_{t=1}^{T} n_{i,k}^2(t)}$, where $n_{i,k}$ is a single regressor time course, i is the index over multiple regressors and N_R is the total number of regressors. Finally, we concatenated the corresponding total nuisance norms across different scans to obtain a nuisance norm vector as $|n|_{\text{Vec}} = \{|n_1|, |n_2|, \ldots, |n_k|, \ldots, |n_K|\}$.

2.5. Nuisance contamination maps: nuisance contamination of FC estimates across scans

We quantify the nuisance contamination in inter-scan FC estimates by correlating the nuisance norm vectors $|n|_{\text{Vec}}$ with the vector of FC estimates FC_{Vec} for each seed-voxel pair. This approach is illustrated in Fig. 1. In the top row, we first computed the correlations between a seed signal (e.g. PCC seed shown with red color) and the time series from every other voxel (lines with blue color) to form a seed-based correlation map for each scan (represented as a $N \times 1$ column vector with red color). We then repeated this for all 68 scans and concatenated the resulting seed-based correlation vectors (FC maps) to form a $(N \times 68)$ matrix as shown in the left hand side in the second row. Each row of this matrix corresponds to the FC estimates vector for a single seed voxel pair (an example row is shown with green color). We then computed the correlations between the FC estimates rows and nuisance norm vector (time series with black color) to form a nuisance contamination vector which can be reshaped into a 3D nuisance contamination map. The green colored square in the nuisance contamination vector corresponds to a single correlation coefficient obtained between the nuisance norm and the FC vector from a single seed voxel pair. This is also depicted on the nuisance

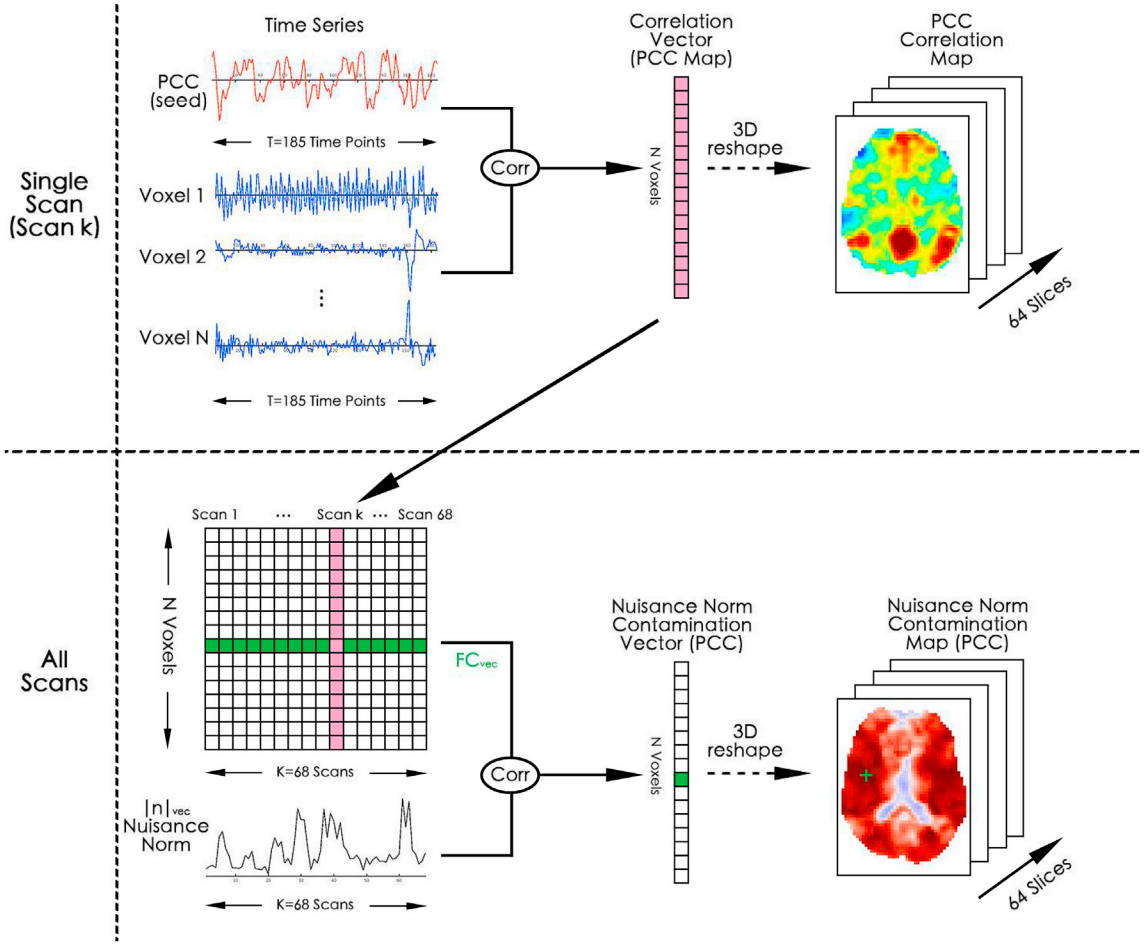

Fig. 1. Diagram illustrating how to obtain nuisance contamination maps. These maps visualize the spatial distribution of the correlations between inter-scan FC estimates (FC_{Vec}) and nuisance norms ($|n|_{\text{Vec}}$). In the first row, a seed signal (e.g. PCC seed) is correlated with signals from other voxels in the brain to form a vector (vertical vector with red color) of FC estimates. This vector represents the canonical seed-based PCC correlation map. This step is repeated across all 68 scans and the resulting PCC maps are concatenated column-wise to form a matrix of FC estimates across scans. This matrix is shown on the bottom left-hand side. The individual rows of the matrix correspond to inter-scan variations in the FC between the PCC seed and a single voxel (an example is shown with green color). Each column is the PCC map for a single scan. The individual rows of this matrix are then correlated with the nuisance norm (shown at the bottom left) to obtain the nuisance contamination values as a 1D vector. An entry of the nuisance contamination vector corresponds to the correlation between the nuisance norm and the FC vector from a single seed-voxel pair. This is illustrated with the dark green (+) symbol on the contamination map. The nuisance contamination vector can be reshaped into a 3D volume to investigate regions of nuisance contamination across the brain.

contamination map with the green (+) symbol.

We obtained nuisance contamination maps both before and after each regression and for different seed signals including the PCC, IPS, FEF, MOT, and AUD seeds. Note that these maps are **not** functional connectivity maps, but instead quantify the relations between seed-based FC estimates and nuisance norms across different scans.

2.6. Theoretical bound on ΔFC

In Nalci et al. (2019) we presented a theoretical expression for the difference ΔDFC = (Post DFC − Pre DFC) between the dynamic FC (DFC) estimates obtained before and after nuisance regression in seed correlation-based DFC studies. This mathematical theory applies for static FC studies as well by noting that a temporal sliding window in DFC analysis can be replaced by the whole scan duration. Thus, the following theoretical bounds apply for the difference between Pre FC and Post FC estimates obtained before and after nuisance regression:

$$\left|\Delta\text{FC}\right| = \left|\text{Post FC} - \text{Pre FC}\right| \leq 2\left(\frac{1-\sqrt{\left|n_O\right|^2/\left|n\right|^2}}{1+\sqrt{\left|n_O\right|^2/\left|n\right|^2}}\right) \tag{1}$$

Here, n is a single nuisance regressor time course represented in vector notation. The nuisance regressor can be decomposed as $n = n_I + n_O$, where n_I is an in-plane component that lies in the subspace spanned by a single seed-voxel pair x_1 and x_2, and n_O is the component orthogonal to this subspace.

The orthogonal nuisance fraction $0 \leq \frac{\left|n_O\right|^2}{\left|n\right|^2} \leq 1$ reflects the nuisance energy that lies in the orthogonal subspace and serves as a measure of orthogonality between the nuisance regressor and the seed-voxel pair (e.g. x_1 and x_2). If n_O becomes arbitrarily large then the fraction $\frac{\left|n_O\right|^2}{\left|n\right|^2} \to 1$ and $|\Delta\text{FC}| \to 0$. An example of this bound is provided in Fig. 5 where a large orthogonal nuisance fraction for the HM, WM, CSF and HM+WM+CSF regressors impose a narrow bound on $|\Delta\text{FC}|$ values forcing them to cluster close to 0.

Note that an exact value for the orthogonal nuisance fraction $\frac{\left|n_O\right|^2}{\left|n\right|^2}$ can be obtained when using a single regressor such as the GS. In the case of multiple regressors, an estimate of the orthogonal nuisance fraction and $|\Delta\text{FC}|$ can be obtained by using the first principal component (PC) of the multiple regressors as in Nalci et al. (2019). This simple approximation enables us to understand the approximate relation between $|\Delta\text{FC}|$ and the orthogonal nuisance fraction. When we analyze multiple regressors, we will provide the approximate orthogonal nuisance fraction values and will also show that regression with the first PC is a good approximation to performing multiple regression.

2.7. Significance testing of the relation between FC variations and nuisance norms across scans

We assessed the statistical significance of the relation between the FC estimates and nuisance norms across scans using non-parametric null testing. As the ordering of scans is not important, we formed null distributions by randomly permuting the scan ordering of FC estimates for each seed voxel pair and nuisance norm over 10,000 trials. We then correlated the resulting surrogate FC estimates with nuisance norms and obtained 10,000 null correlation values both before and after nuisance regression. We used the null distributions to assess the statistical significance of the correlations between the non-permuted FC estimates and nuisance norms.

3. Results

In this section we show that variations in FC estimates across multiple scans are significantly correlated with the geometric norms of various nuisance terms. We demonstrate that a considerable portion of the FC estimates remains significantly correlated with nuisance norms even after nuisance regression. We make use of the theoretical findings from Nalci et al. (2019) to show that the inefficacy of nuisance regression for non-GS regressors such as HM, WM and CSF is largely due to the large orthogonality between nuisance regressors and the BOLD data within each scan. We further show that GSR can introduce negative GS norm fluctuations into the FC estimates.

Before proceeding, it is useful to provide some context for the results by reviewing the key observation made in (Nalci et al., 2019): *the nuisance norm can be highly correlated with the FC estimates across time windows (for DFC) or scans (for static FC) even though the correlation of the nuisance term with the underlying time series can be quite low*. This is because each nuisance term can be decomposed into an *in-plane* component n_I that lies in the sub-space spanned by the pair of fMRI signals $x_{1,k}$ and $x_{2,k}$ under consideration and an *orthogonal* component n_O that is perpendicular to the sub-space. Variations across scans in the length (i.e. norm) of the in-plane component can give rise to variations in the FC estimates, such that the in-plane norm $|n_I|$ is correlated with the FC estimates over scans. If the norms ($|n_I|$ and $|n_O|$) of the in-plane and orthogonal components vary in the roughly the same manner across scans, then the overall nuisance norm $|n|$ will also be correlated with the FC estimates across scans. However, if the orthogonal component is relatively large with an orthogonal nuisance fraction $\left|n_O\right|^2/\left|n\right|^2$ that is close to 1, then the overall nuisance component in any given scan will be largely orthogonal to the underlying fMRI signals. When this is the case, regression will have relatively little effect on the underlying fMRI signals due to the high degree of orthogonality. As a result, the FC estimates will also be largely unaffected by regression. For additional explanations and some simple toy examples, the motivated reader is encouraged to consult the Interpretation section of (Nalci et al., 2019).

In the first row of Fig. 2 we show examples of the relation between nuisance norms and FC estimates for 3 seed pairs: PCC&AUD, MPF&AUD and PCC&IPS. The column labels indicate both the type of nuisance norm and the specific seed-pair. The FC estimates in each column (blue lines, labeled as Pre FC) are significantly ($p < 10^{-3}$) correlated with various nuisance norms (black lines) before nuisance regression. The correlations obtained between the Pre FC estimates and HM, HM+WM+CSF, and GS norms in the first, second, and third columns are $r = 0.56$, $r = 0.58$, and $r = 0.82$, respectively. After nuisance regression, the Post FC estimates are still significantly correlated with the nuisance norms with correlations of $r = 0.50$, $r = 0.55$, and $r = 0.54$ observed for HM, HM+WM+CSF, and GS norms, respectively. The second row shows the same relations using scatter-plots where the FC estimates are plotted against the respective nuisance norms.

The results presented below generalize the relation between various nuisance norms and PCC-based FC estimates to include all PCC seed-voxel pairs. We provide the results for other seeds in the supplementary material and main text below.

3.1. HM regression

In Fig. 3a and b we show the PCC-based HM contamination maps before and after HM regression. These maps are very similar to each other (cosine similarity $S = 0.98$) and show widespread correlations between the HM norm and FC estimates across scans both before and after HM regression.

In the scatter plot shown in Fig. 4 we plot the correlations obtained between the Post FC estimates and HM norm versus the correlations obtained between the Pre FC estimates and HM norm. The sideways histogram along the y-axis shows the distribution of correlation values obtained between the Post FC estimates and HM norm, which ranged from $r = -0.36$ to $r = 0.60$ with a mean of 0.27. The histogram along the x-axis at the bottom shows the correlations obtained between the Pre FC

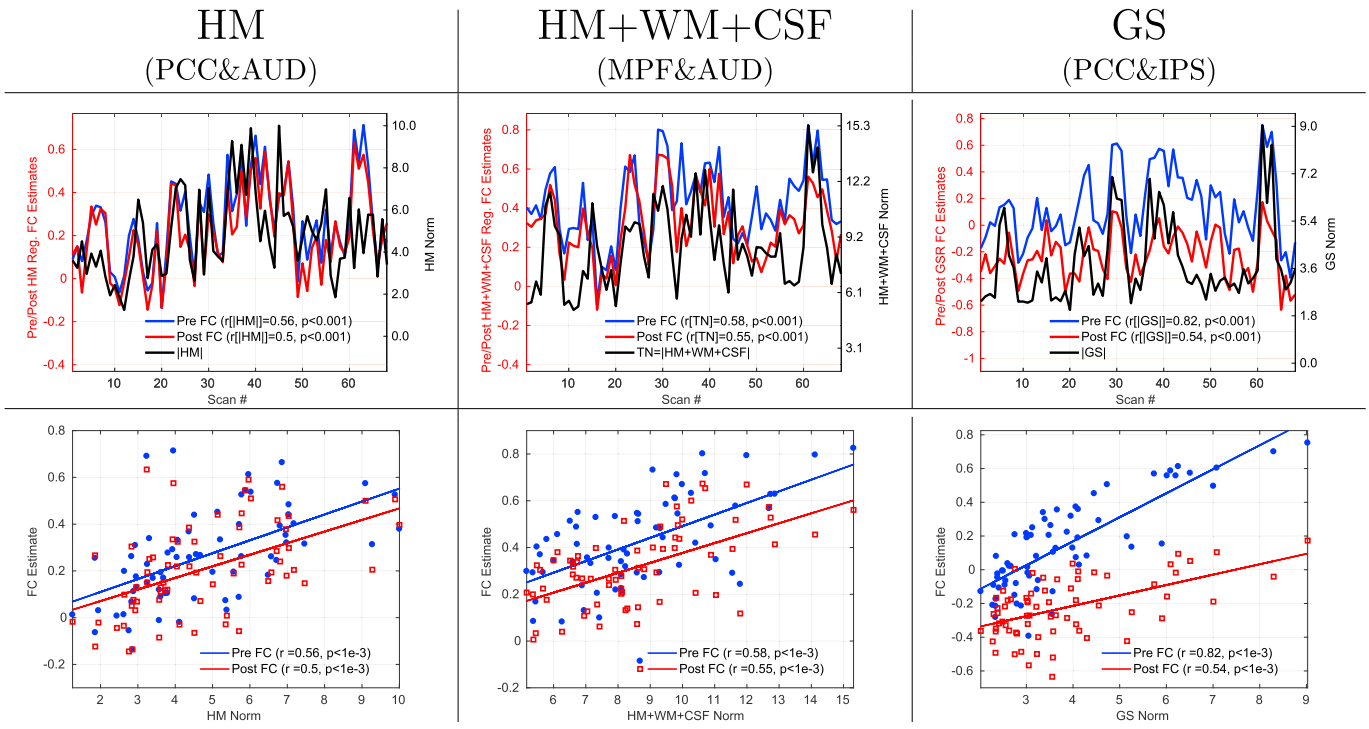

Fig. 2. FC estimates obtained from 3 example seed pairs both before (blue lines) and after (red lines) nuisance regression are significantly correlated ($p < 10^{-3}$) across scans with various nuisance norms (black lines). The type of nuisance norm and seed pair are indicated by the column labels. In the first row the FC estimate values are indicated on the left y-axis in each column, nuisance norm values are indicated on the right y-axis, and scan numbers are indicated by the x-axis. Before nuisance regression, the correlations between the Pre FC estimates and nuisance norms were $r = 0.56$, $r = 0.58$, and $r = 0.82$ for the HM, HM+WM+CSF, and GS norms, respectively. After nuisance regression, the correlations between the Post FC estimates and nuisance norms were $r = 0.50$, $r = 0.55$, and $r = 0.54$ for the HM, HM+WM+CSF and GS norms, respectively. The first row serves as a nice visual demonstration of the similarity between the fluctuations in nuisance norms and FC estimates. The second row shows the relation between the FC estimates and nuisance norms using scatter-plots.

estimates and HM norm, which ranged from $r = -0.34$ to $r = 0.61$ with a mean of 0.26. These two correlation distributions were strongly related to each other ($r = 0.94, p < 10^{-3}$). The linear fit (blue line) between the correlation distributions (Slope = 0.91, Offset = 0.04) was very close to the line of unity (yellow dashed line). This indicates that HM regression had a very limited effect in removing the correlations between the Pre FC estimates and HM norms, and the correlations with the HM norm largely persisted after HM regression.

As shown in Table 1, 45% of the PCC-based Pre FC estimates were significantly correlated ($p < 0.05$) with HM norms. We further computed the mean and standard deviation of the percent variance explained by the HM norm for those significant 45% Pre FC estimates. The HM norm explained an average of 11%±4% (mean±SD) of the variance in those significant Pre FC estimates. After HM regression, 51% of the Post FC estimates were significantly correlated with the HM norm. The HM norm explained an average of 11%±4% (mean±SD) of the variance in those Post FC estimates, which is the same percent variance explained prior to HM regression.

Ideally, HM regression should fully remove the HM norm variance from the Post FC estimates. However, from Fig. 4 we see that the Post FC estimates are still correlated with HM norm nearly as much as the Pre FC estimates are correlated with HM norm. In Fig. 5a we show the theoretical limitation of HM regression. Each point in this plot shows the ΔFC (difference between the Pre FC and Post FC estimates) versus the orthogonal nuisance fraction $|n_O|^2 / |n|^2$ for a single seed-voxel pair in a single scan. The HM regressors are largely orthogonal to most seed voxel pairs across scans with a mean orthogonal fraction of $|n_O|^2 / |n|^2 = 0.99$. Due to the large orthogonal fraction, the theoretical bounds force the ΔFC values to be clustered around a mean value of 0. Since HM regression cannot really alter the Pre FC estimates, the slope of the linear fit in Fig. 4 remains close to the line of unity.

Note that as in Nalci et al. (2019) we used the first principal component (PC) across all head motion measurements for the ΔFC plot in Fig. 5a. We provide the ΔFC plot after performing multiple HM regression in Supplementary Fig. 1, which shows that ΔFC values are still largely clustered around zero (mean ΔFC = − 0.037), roughly within the tight theoretical bounds.

We present the HM contamination maps and their respective correlation distributions before and after HM regression for other seeds (e.g. MOT, AUD, FEF, and IPS) in Supplementary Figs. 3–6. These were similar to the PCC-based results discussed above. Additionally, Table 1 summarizes the significance results of the relation between nuisance norms and FC estimates for other seeds.

3.2. HM+WM+CSF regression

In Fig. 6a and b we show the HM+WM+CSF contamination maps both before and after nuisance regression. These maps show widespread correlations between the nuisance norm and FC estimates across scans. In panel (b) there is a visible reduction in the positive correlation values (i.e. red regions) after regression with a slight increase in anti-correlations (i.e. blue regions start to appear).

In Fig. 6c the correlations between the Pre FC estimates and nuisance norm ranged from $r = -0.26$ to $r = 0.81$ with mean 0.46. After nuisance regression, the correlation between the Post FC estimates and nuisance norm ranged from $r = -0.42$ to $r = 0.66$ with mean 0.23. We found a strong linear relation between the two correlation distributions ($r = 0.82$, $p < 10^{-3}$) with a slight increase in significant anti-correlations residing below the lower red significance line. The linear fit between the two correlation distributions was close to the line of unity with a large slope (0.83) and a small negative offset (− 0.15).

As noted in Table 1, 88% of the Pre FC estimates were significantly

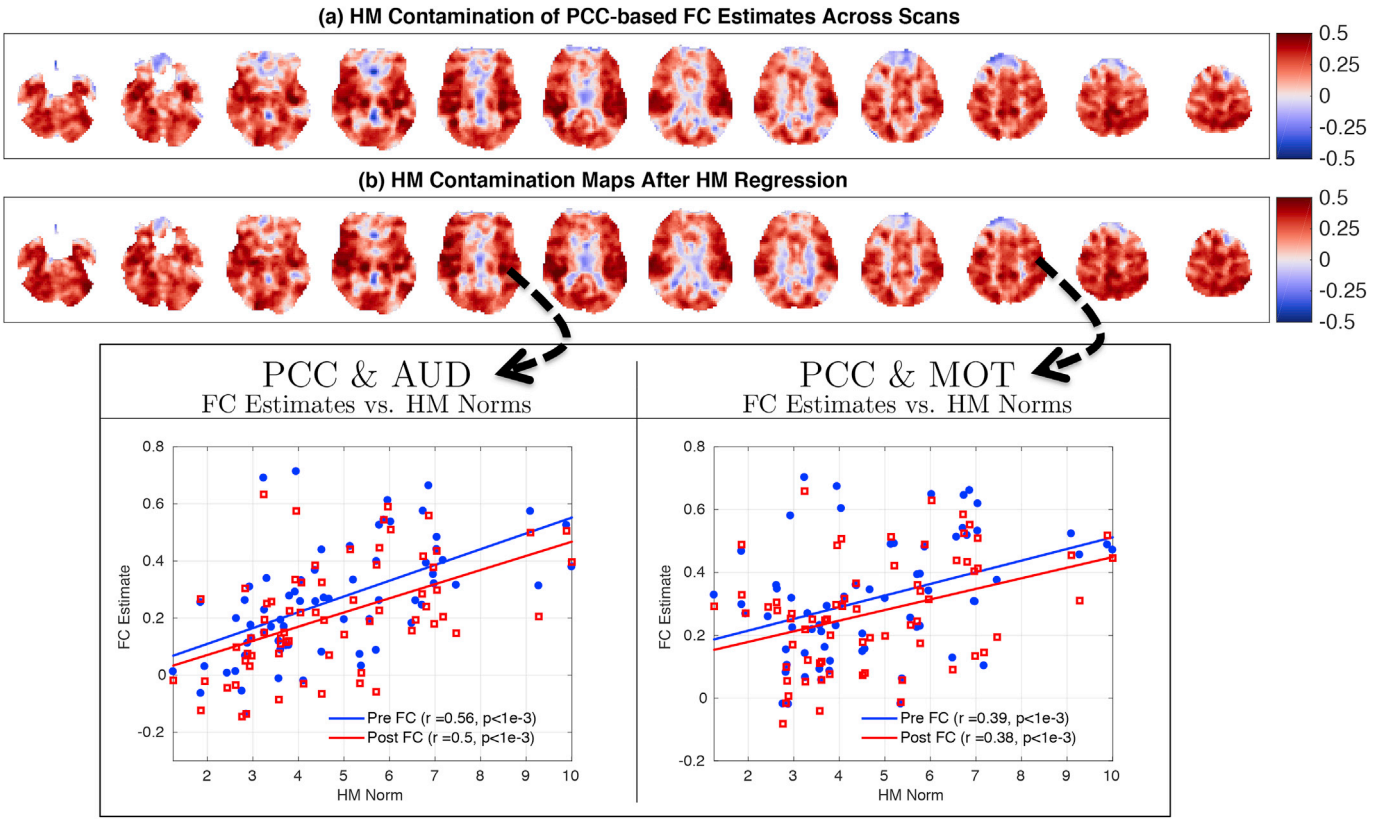

Fig. 3. HM contamination maps obtained by correlating the HM norm with FC estimates (a) before and (b) after HM regression. The contamination maps in (a) and (b) are fairly similar to each other (cosine similarity $S = 0.98$) and both show widespread correlations between the HM norm and FC estimates across scans. This indicates that HM regression is largely ineffective in removing the relation between the HM norm and FC estimates. We show two example seed-pairs (PCC & AUD and PCC & MOT) at the bottom to illustrate the relation between HM norms and FC estimates for two different regions.

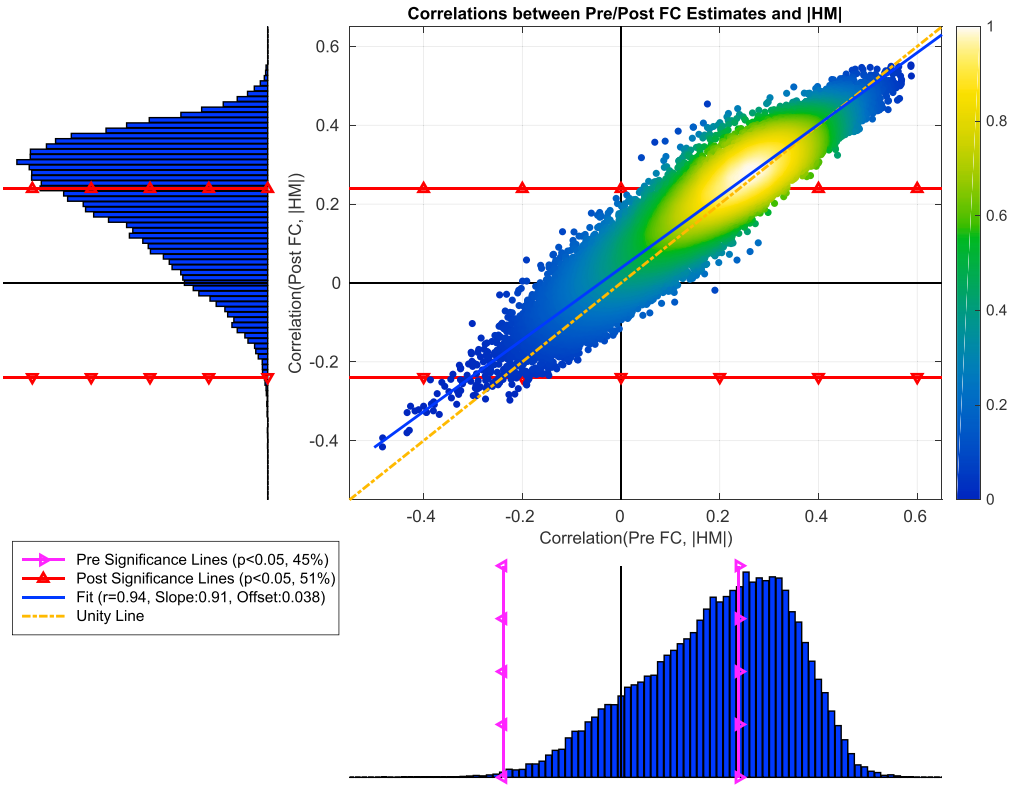

Figure 4. The correlations between the Post FC estimates and HM norm versus the correlations obtained between Pre FC estimates and HM norm. These correlation distributions were significantly related ($r = 0.94$, $p < 10^{-6}$) to each other. The linear fit (blue line, Slope$= 0.91$ and Offset$= 0.04$) between the two correlation distributions was fairly close to the line of unity (dashed yellow line). At the bottom histogram, the correlations between the Pre FC estimates and HM norms ranged from $r = -0.34$ to $r = 0.61$ with mean 0.26. We superimposed the significance lines ($p < 0.05$) on this histogram using magenta lines with triangles (labeled as Pre Significance). Based on the significance line, 45% of the Pre FC estimates were significantly correlated with HM norms. In the sideways histogram to the left, the correlations between the Post FC estimates and HM norms ranged from $r = -0.36$ to $r = 0.60$ with mean 0.27, where significance lines are shown with red lines with triangles. 51% of the Post FC estimates were significantly correlated with HM norms after HM regression.

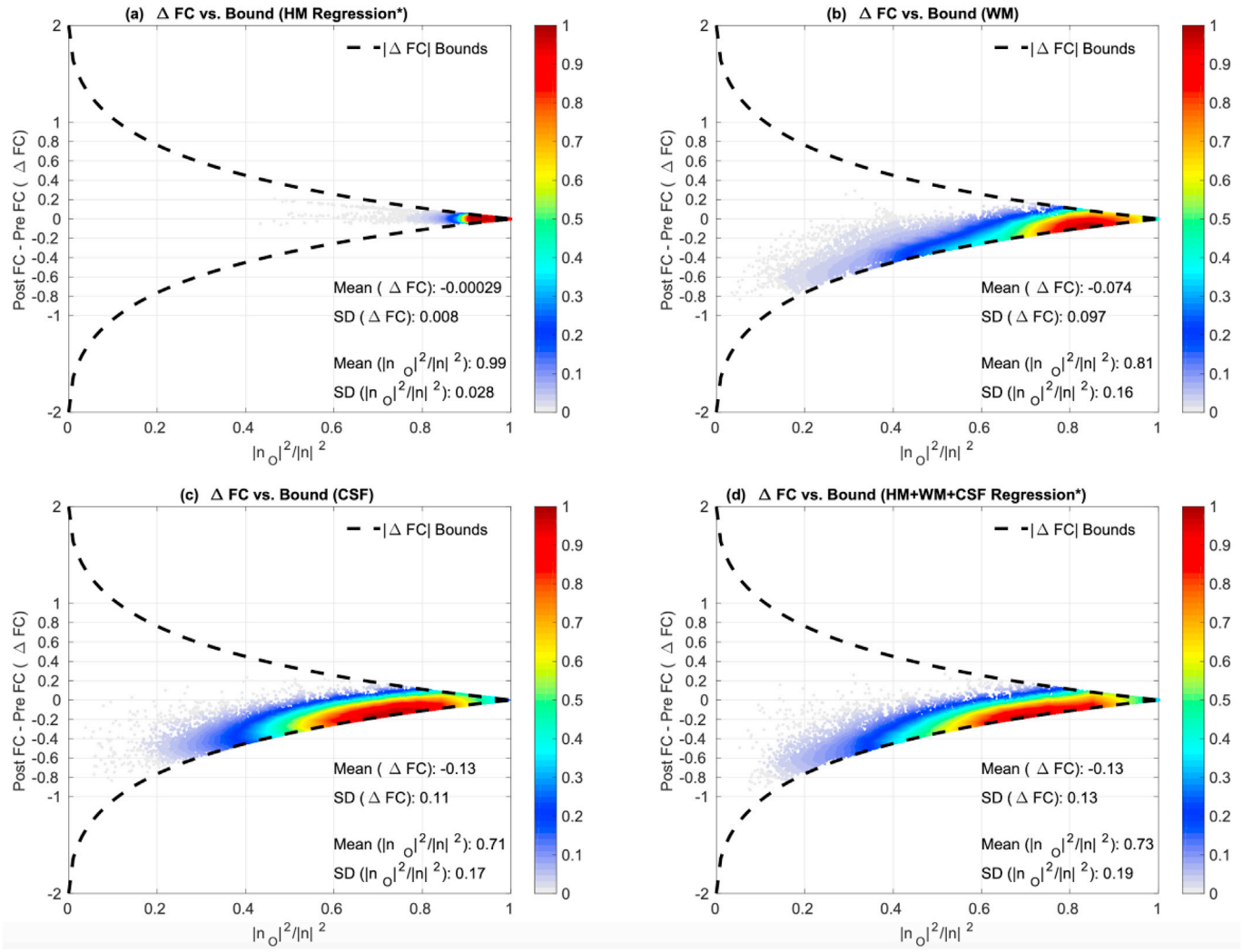

Fig. 5. ΔFC versus orthogonal nuisance fraction $\frac{|n_O|^2}{|n|^2}$ for HM (1st PC), WM, CSF and HM+WM+CSF (1st PC) regressor groups. Each point in these plots represent the values for a single scan and a single seed-voxel pair. In (a) we plot the ΔFC versus the orthogonal nuisance fraction for HM regression. We see that the points are strictly clustered on the right hand side around a mean orthogonal nuisance fraction value of 0.99. This imposes an extremely tight bound on the ΔFC values before and after HM regression, resulting in a negligible effect on the FC estimates (mean ΔFC = 0). In (b), (c) and (d) we plot the ΔFC versus the orthogonal nuisance fraction for the WM, CSF, and 1st PC of HM+WM+CSF regressors, respectively. These regressors are largely orthogonal to the seed-voxel pair time series data with mean orthogonal fractions $\frac{|n_O|^2}{|n|^2} > 0.70$, resulting in fairly tight bounds on the ΔFC values. Thus, the effects of these regressors on the FC estimates are very limited with mean $|\Delta FC| \leq 0.13$.

Table 1
Summary of the relationship between the FC estimates and nuisance norms obtained before and after nuisance regressions for 5 seed signals. The seed signal and regression state (e.g. before and after) are indicated in the first and second columns, respectively. For each nuisance regression we report the percentage of seed-voxel pairs for which there was a significant correlation between the FC estimates and nuisance norms. We also provide the mean and standard deviation of the percent variance explained in the FC estimates by the nuisance norms over the respective subsets of significant seed-voxel pairs.

Seed	State	HM		HM+WM+CSF		GS		HM+WM+CSF+GS	
		%Brain	%Var mean±SD	%Brain	%Var mean±SD	%Brain	%Var mean±SD	%Brain	%Var mean±SD
PCC	Pre FC	45	11±4	88	27±12	96	37±15	91	31±14
	Post FC	51	11±4	56	13±6	27	11±5	26	11±5
MOT	Pre FC	45	13±5	96	26±9	99	38±13	98	30±10
	Post FC	49	13±5	74	15±7	30	13±6	20	11±5
AUD	Pre FC	60	13±5	98	28±10	99	40±13	98	33±12
	Post FC	63	14±6	75	16±8	25	11±5	22	10±4
FEF	Pre FC	43	11±4	100	32±9	99	49±11	99	38±10
	Post FC	49	11±4	82	17±8	24	11±5	23	11±5
IPS	Pre FC	40	11±4	97	25±9	99	40±13	98	29±10
	Post FC	43	11±4	63	13±6	20	12±5	23	11±5

correlated ($p < 0.05$) with the nuisance norm. The nuisance norm explained an average of 27%±12% (mean±SD) of the variance in those significant correlations. After regression, 56% of the Post FC estimates were still significantly correlated with the nuisance norm, and the nuisance norm explained an average of 13%±6% (mean±SD) of the variance in those Post FC estimates.

In Fig. 5b and c we show the ΔFC plots for the WM and CSF regressors. We found that the mean orthogonal nuisance fraction for the WM and CSF regressors were still relatively large with $|n_O|^2/|n|^2 = 0.81$ and $|n_O|^2/|n|^2 = 0.71$, respectively. Due to the theoretical bounds associated with the large orthogonal fractions, the ΔFC points were clustered close to 0 with mean ΔFC values of −0.08 and −0.13 for the WM and CSF regressors, respectively. In Fig. 5d we show the ΔFC plot for the HM+WM+CSF regression using the first PC of those regressors. This revealed a mean orthogonal fraction of $|n_O|^2/|n|^2 = 0.73$ (similar to individual WM and CSF regressors) with mean ΔFC around −0.13 and ΔFC values bounded below by the theoretical bound. In Supplementary Fig. 2, we show that the 'true' ΔFC values (i.e. not approximated with the 1st PC) lie within a fairly narrow neighborhood around the theoretical bounds with a mean ΔFC = − 0.17, similar to Fig. 5d.

To summarize, although HM+WM+CSF regression partially reduced the correlations between the nuisance norm and Pre FC estimates (as compared to HM regression alone), a large fraction of seed-voxel pairs (56%) exhibited significant correlations between the nuisance norm and Post FC estimates. The limited efficacy of nuisance regression reflects the fact that the theoretical bounds on ΔFC estimates in Fig. 5d are still very tight since the orthogonal nuisance fraction is large and close to 1.0.

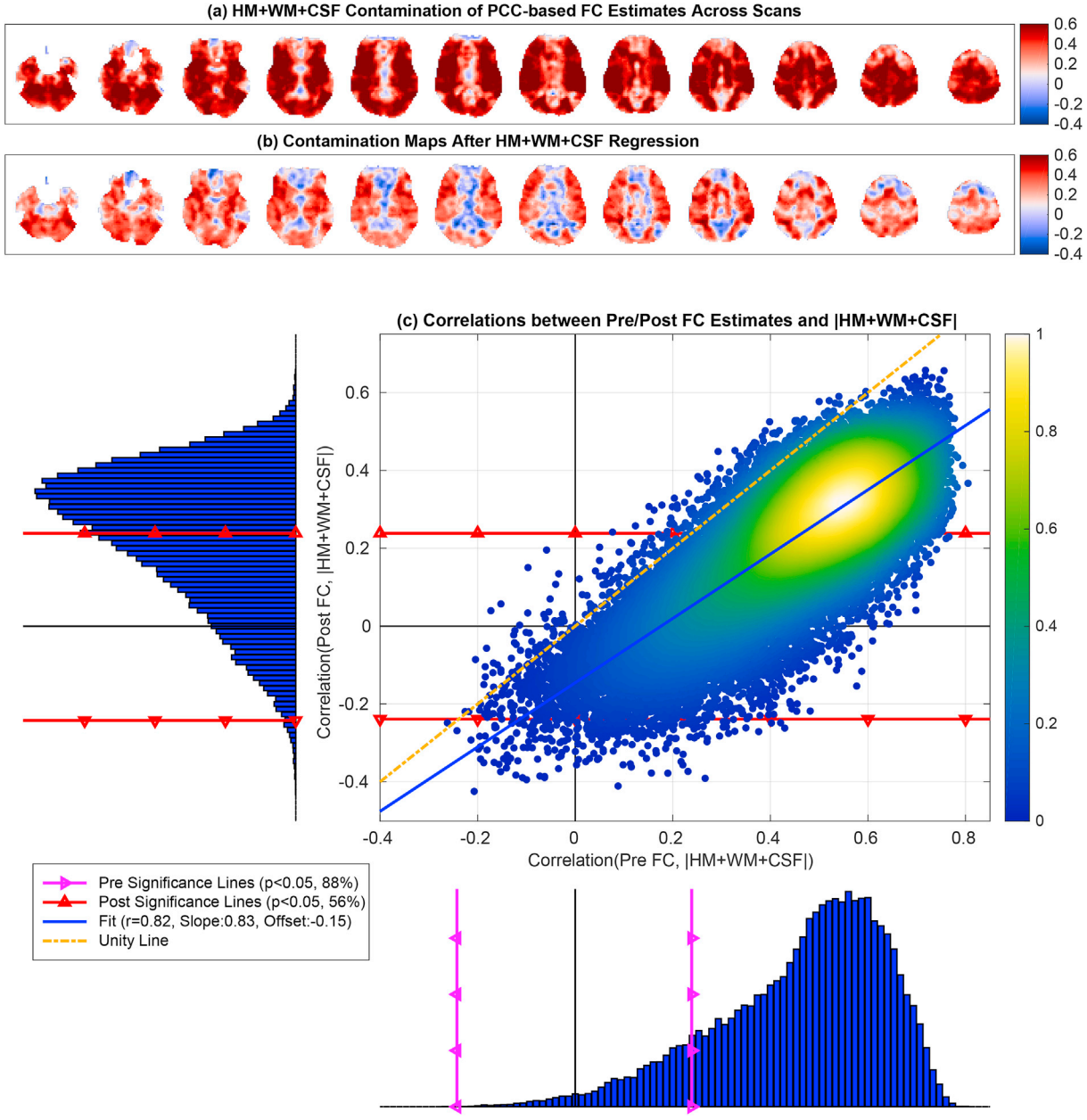

Fig. 6. Nuisance contamination maps obtained by correlating the total HM+WM+CSF norm with the FC estimates (a) before and (b) after nuisance regression. In (c) the correlations between the Pre FC estimates and the nuisance norm (x-axis) ranged from = −0.26 to $r = 0.81$ with mean 0.46. The correlations between the Post FC estimates and nuisance norm (y-axis) ranged from = −0.42 to $r = 0.66$ with mean 0.23. There was a strong linear relation between the two correlation distributions (linear fit $r = 0.82, p < 10^{-6}$). The linear fit between the two correlation distributions was close to the line of unity with a large slope (0.83) and a small negative offset (− 0.15).

We present the HM+WM+CSF contamination maps and their respective correlation distributions before and after nuisance regression for other seeds (e.g. MOT, AUD, FEF, and IPS) in Supplementary Figs. 7–10. These were similar to the PCC-based results discussed above. Additionally, Table 1 summarizes the relations between nuisance norms and FC estimates for other seeds.

3.3. GS regression

In Fig. 7a and b we show GS contamination maps both before and after GSR. In panel (a) we observe strong positive correlations (red regions) between the GS norm and Pre FC estimates. The distribution of these correlations is shown in Fig. 8, with values ranging from $r = -0.22$ to $r = 0.87$ with mean 0.57. Across the sample, 96% of these correlations were significant ($p < 0.05$) and 99% were positive with a strong left skew $S = -0.96$. The GS contamination map after GSR is given in Fig. 7b. This map shows brain regions consisting of both positive (red regions) and anti-correlations (blue regions) between the GS norms and Post FC estimates.

In Fig. 7b we observe that GSR introduces anti-correlations between the GS norm and FC estimates which were not present prior to GSR in panel (a). An example seed pair is provided at the bottom of Fig. 7 as a scatter plot. The FC estimates obtained between the PCC&MPF seeds on the left-hand side are positively correlated with the GS norm before GSR and anti-correlated with the GS norm after GSR. As shown along the y-axis of Fig. 8 the correlations between the GS norm and Post FC estimates ranged from $r = -0.61$ to $r = 0.66$ centered around a mean of 0 with standard deviation 0.21. 49% of these correlations were positive (remaining 51% were negative) and 27% were significant ($p < 0.05$).

In Fig. 8 we found a significant linear relationship ($r = 0.59$, $p < 10^{-6}$) between the correlations obtained between the Post FC estimates and GS norm versus those correlations obtained before GSR. The linear fit (shown with the blue line) is fairly parallel to the line of unity (green dashed line) with a slope of 0.77 and has a very large negative offset -0.44. The negative offset indicates that GSR produces a strong negative shift in the correlations obtained between the Post FC estimates and GS norms when compared to those correlations obtained before GSR. This results in significant anti-correlations ($p < 0.05$) between the GS norms and Post FC estimates. The significant anti-correlations between the GS norms and Post FC estimates are shown with the points residing below the bottom significance line (red line with triangles) within the dark blue zone in the scatter plot. The points residing above the top significance line in the dark red zone are significant positive correlations remaining after GSR. These correlation values remain significant and positive despite the negative offset.

These results indicate that effects related to the GS norm can largely remain in the Post FC estimates after GSR. GSR can result in "residual" positive correlations between the GS norm and Post FC estimates and can also "introduce" significant anti-correlations between the GS norm and Post FC estimates due to the negative shift in correlation values. To understand why GSR results in both positive and negative correlations between the GS norm and Post FC estimates we start by defining two zones as illustrated in Fig. 8 with dark red and dark blue zones labeled by *Zone I* and *Zone II*.

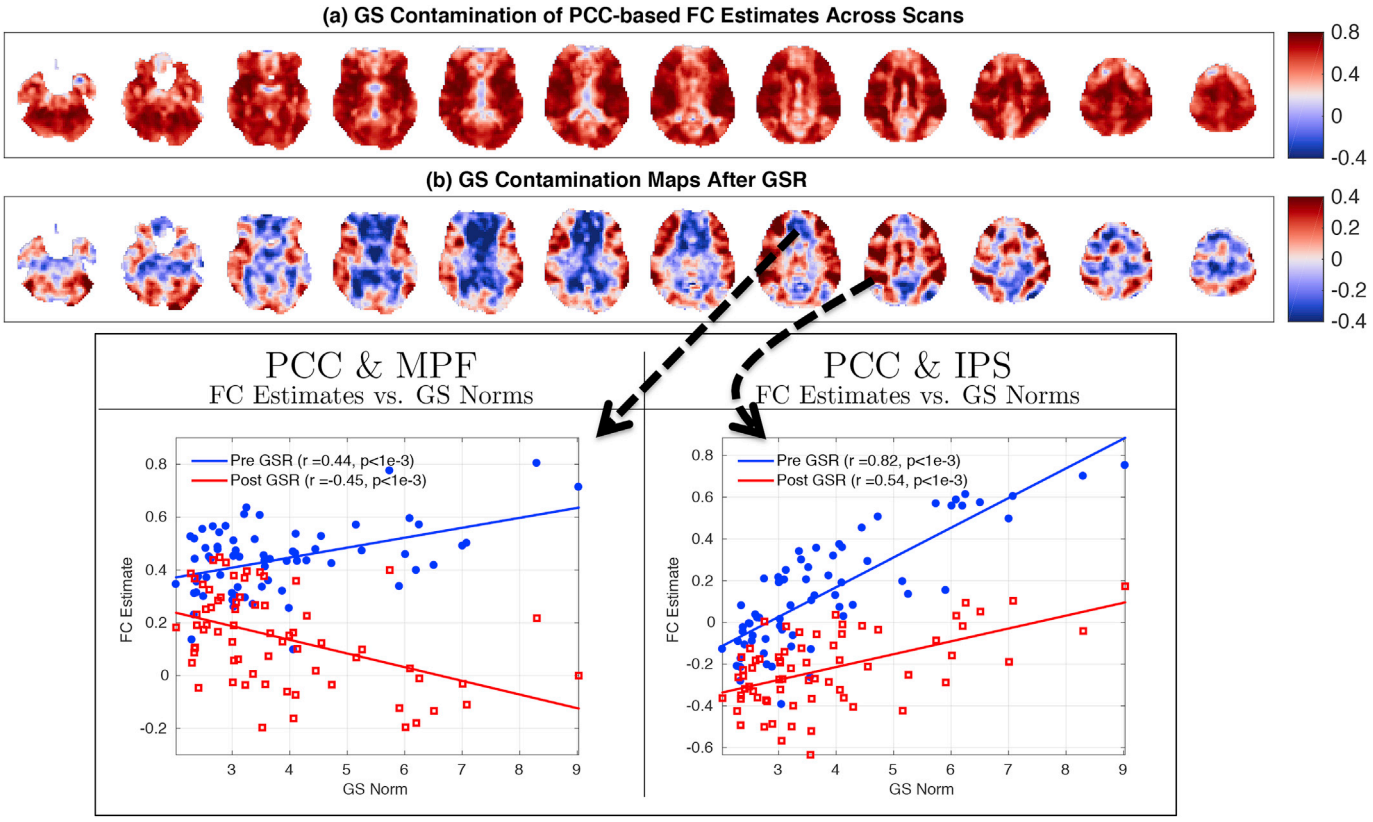

Fig. 7. GS contamination maps obtained both (a) before and (b) after GSR. In panel (a) the contamination maps show positive and significant correlations (99% positive and 96% significant) between Pre FC estimates and GS norm. In (b) the contamination map after GSR exhibits both positive (49%) and negative (51%) correlations between the GS norms and Post FC estimates. 27% of these correlations were significant ($p < 0.05$). In the seed-pair examples shown at the bottom, the FC estimates between the PCC & MPF across scans are positively correlated with GS norms before GSR ($r = 0.44$) but become anti-correlated after GSR ($r = -0.45$). The FC estimates for the PCC & MPF seed pair are positively correlated with the GS norm both before and after GSR with correlation values of $r = 0.82$ and $r = 0.54$, respectively.

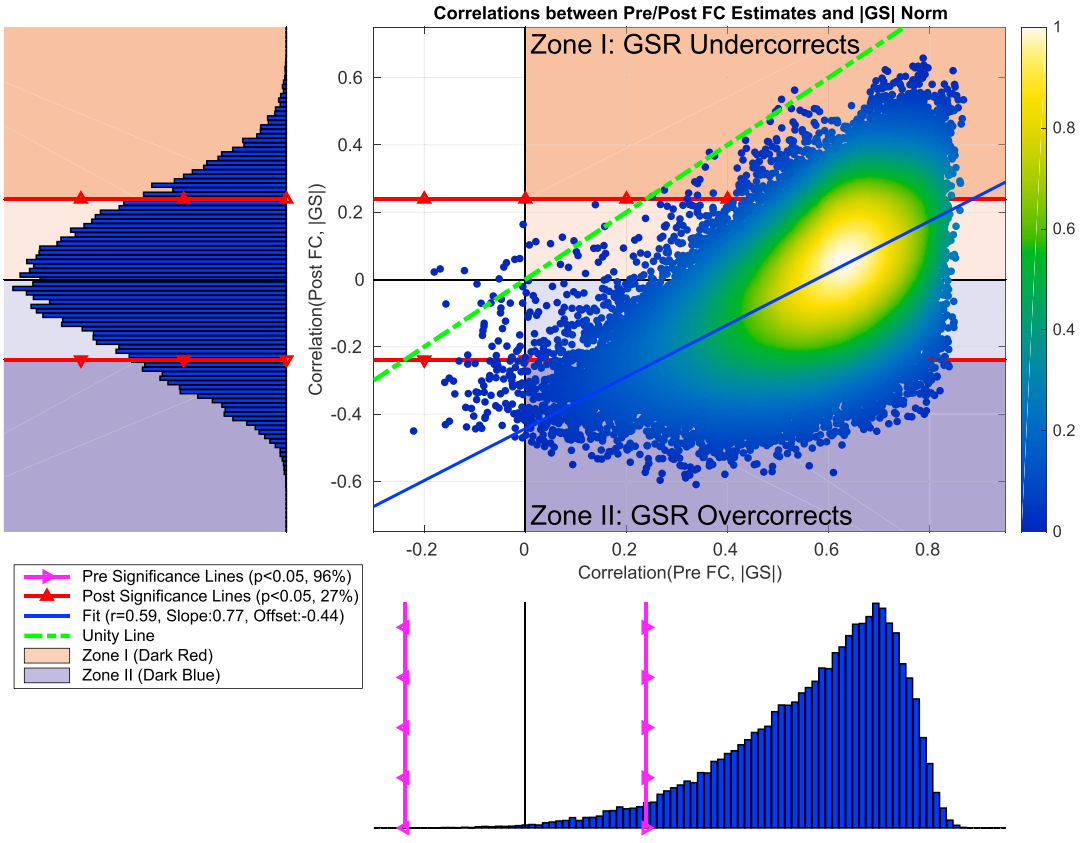

Fig. 8. In the scatter plot, we show the correlations between the Post FC estimates and GS norms plotted versus the correlations obtained between the Pre FC estimates and GS norms. We found a significant linear relationship between the two correlation distributions ($r = 0.59, p < 10^{-6}$). The linear fit (blue line) had a slope of 0.77 and a very large negative offset -0.44. In the bottom histogram, the correlations between the Pre FC estimates and GS norms ranged from $r = -0.22$ to $r = 0.87$ with mean 0.57 and standard deviation 0.16. 99% of the correlations were positive with a strong left skew (Skewness $= -0.96$) and 96% of the correlations were significant ($p < 0.05$) (correlations residing to the right of magenta line with triangles). In the sideways histogram on the left, the correlations between the Post FC estimates and GS norm ranged from $r = -0.61$ to $r = 0.66$ with mean 0 and standard deviation 0.21, where significance lines ($p < 0.05$) are shown with red lines with triangles. We found 27% of the Post FC estimates to be significantly correlated with GS norms after regression. The labels on the scatter plot ("Zone I" (red zone) and "Zone II" (blue zone)) refer to two main cases where GSR fails to remove significant correlations between the GS norm and Post FC estimates.

3.3.1. Zone I (GSR undercorrects): GSR is limited in removing GS norm from FC estimates

In Fig. 8, red background colors (both light and dark colors) show those correlations between GS norm and FC estimates that are **positive** both before and after GSR. In this case, GSR undercorrects and is unable to fully remove the positive correlations between the GS norm and FC estimates.

We define Zone I (dark red background) to include the **significant** positive correlations ($p < 0.05$) between GS norm and FC estimates remaining after GSR. In Fig. 9a we plot the average FC estimates (across Zone I seed-voxel pairs) versus the GS norm before GSR (blue line and dots) and after GSR (red line and diamonds), where each point corresponds to a single scan. The correlation between the average Pre FC and GS norm is $r = 0.87$. The correlation between the average Post FC and GS norm after GSR is still large with $r = 0.74$. This indicates that GSR is unable to fully remove the GS norm effects from the Pre FC estimates.

The effect of GSR is fully characterized by the average ΔFC values (black squares) shown in Fig. 9a. The average ΔFC is anti-correlated with the GS norm ($r = -0.81$) where the slope of the linear fit (black line) is -0.068. The slope (0.11) of the linear fit (blue line) between the Pre FC estimates and GS norm has a greater magnitude than the slope (-0.068) for ΔFC. Since Post FC = Pre FC + ΔFC, this difference in the slope magnitudes results in a positive slope for the relation between Post FC estimates and GS norm (linear fit shown with red line).

In Fig. 10a we plot the ΔFC values versus orthogonal nuisance fraction for Zone I, where each point represents the values obtained for a single seed-voxel pair in a given single scan. The ΔFC values are strongly related to the orthogonal nuisance fraction with $r = 0.93$ ($p < 10^{-3}$), where the linear fit shown with the green line is almost tangent to the lower theoretical bound. We observe that ΔFC values are clustered around the lower theoretical bound with mean value of -0.37 with a relatively smaller standard deviation -0.17. This is consistent with the average ΔFC values in Fig. 9a. The bound plot reveals that the effects of GSR on the FC estimates in Zone I are bounded below by the theoretical curve such that the magnitudes of ΔFC cannot exceed the lower bound. As a result, the magnitude of ΔFC in Fig. 9a cannot increase as rapidly as the Pre FC estimates.

3.3.2. Zone II (GSR overcorrects): GSR introduces anti-correlation between GS norm and FC estimates

The light and dark blue backgrounds in Fig. 8 show those correlations between GS norm and FC estimates that are **positive** before GSR and are **negative** after GSR. In this case, GSR overcorrects by first removing the positive correlations between GS norm and Pre FC estimates and then introducing anti-correlations between the GS norms and Post FC estimates. The brain regions which are red in Fig. 7a but are blue in Fig. 7b correspond to this case. These regions broadly include the default mode network, medial-prefrontal cortex, and thalamic regions, when using the

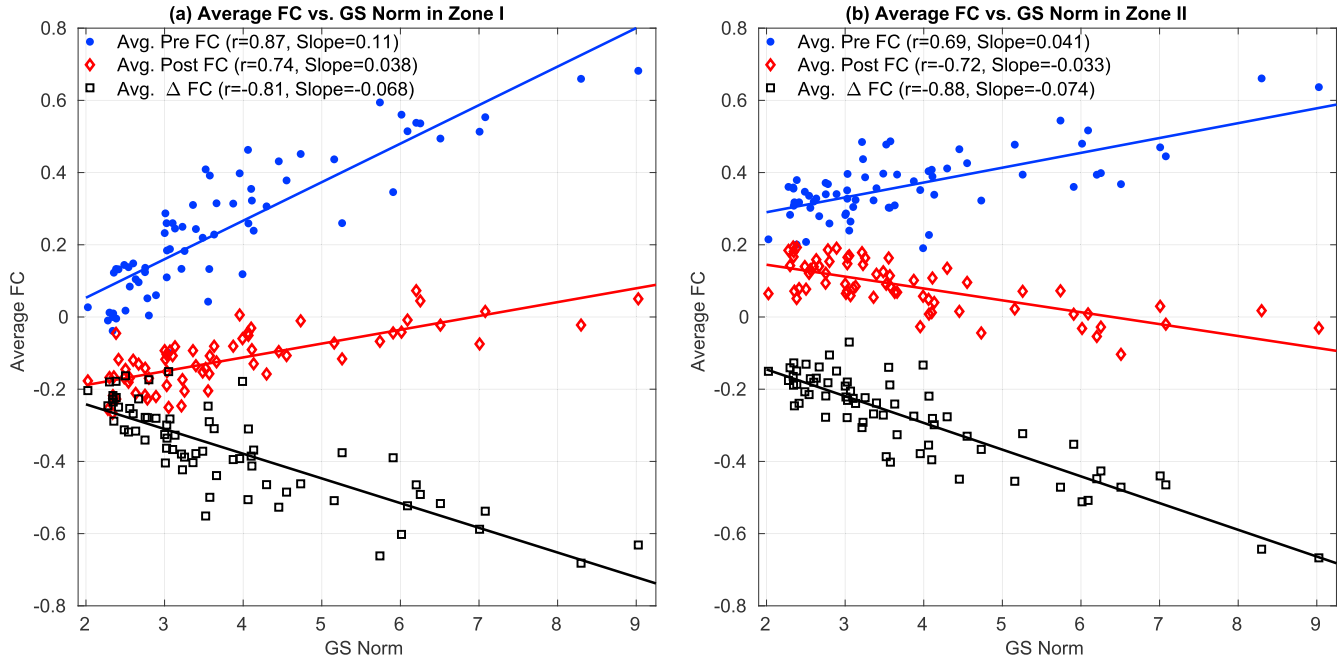

Fig. 9. Average FC estimates and average ΔFC versus GS norm in (a) Zone I and (b) Zone II. In both panels the average effect of GSR is equivalent to adding the average ΔFC (shown with black color) to the average Pre FC estimates (blue color). In Zone 1, the resulting average Post FC estimates (red color) are still positively correlated with the GS norm $r = 0.74$. This is because the slope for average ΔFC (-0.068) has a smaller magnitude than the slope for average FC estimates ($+0.11$). Thus, the slope for average Post FC estimates remains positive $0.038 \approx +0.11 - 0.068$. In panel (b) the average Pre FC estimates for Zone II are significantly larger than those in Zone I in panel (a) $p < 10^{-3}$ (paired two-tailed t-test) with a smaller standard deviation (0.09 in Zone II as compared to the 0.19 in Zone I). Thus, the slope for average Pre FC estimates in Zone II has a smaller magnitude ($+0.041$) as compared to Zone I. The slope (-0.074) of average ΔFC in (b) is similar to the slope (-0.068) of average ΔFC in (a). Since the average Post FC estimates are simply the sum of average Pre FC points and average ΔFC points, the average Pre FC estimates are dominated by the larger ΔFC effect and the relation between the average Post FC estimates and GS norm exhibits a negative correlation ($r = -0.72$, $p < 10^{-3}$).

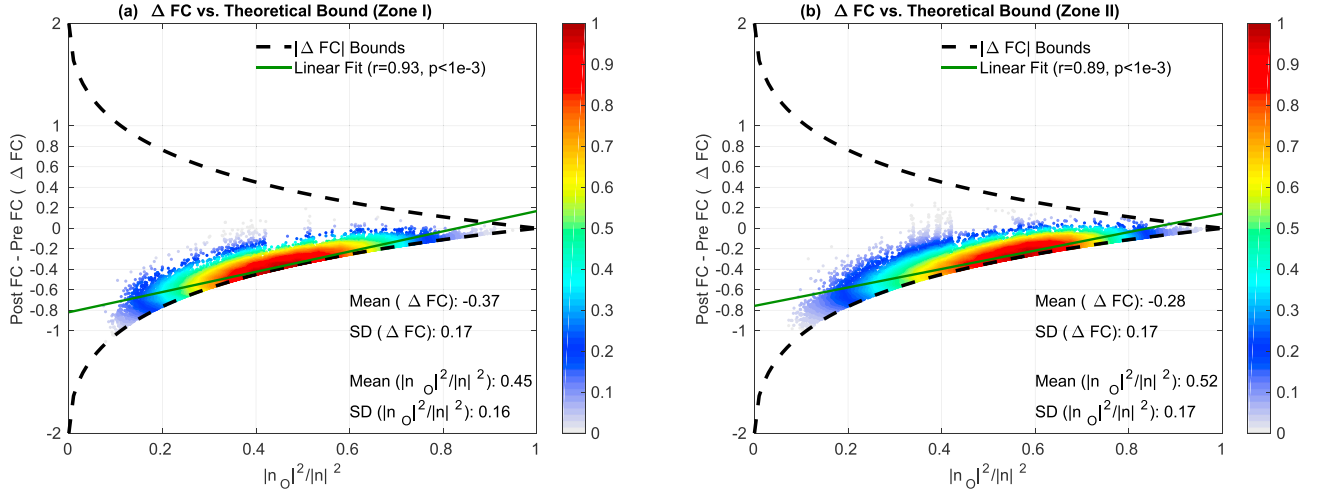

Fig. 10. ΔFC versus orthogonal nuisance fraction $\frac{|n_O|^2}{|n|^2}$ for GS regression in (a) Zone I and (b) Zone II. In both zones, ΔFC values are clustered close to the lower theoretical bound with mean ΔFC values of -0.37 for Zone I and -0.28 for Zone II and similar mean orthogonal nuisance fractions of 0.45 and 0.52, respectively. Moreover, the standard deviations for ΔFC in the two zones are both equal to 0.17, which is much smaller than the mean ΔFC values. The linear fits shown with solid green lines show that ΔFC values are strongly correlated ($p < 10^{-3}$) with the orthogonal nuisance fractions with $r = 0.93$ and $r = 0.89$ for Zone I and Zone II, respectively. Both linear fits are extremely close to the lower theoretical bound.

PCC as the seed signal.

In Fig. 8 we define Zone II (dark blue background) to include **significant** negative correlations ($p < 0.05$) between the GS norm and FC estimates after GSR. In Fig. 9b we plot the average FC estimates versus the GS norm for Zone II. The slope (0.041) of the relation between Pre FC estimates and GS norm in Zone II in Fig. 9b is weaker in magnitude as compared to the slope (-0.074) of the relation between the ΔFC and GS norm. Since Post FC = Pre FC + ΔFC, a stronger negative relation

between ΔFC and GS norm dominates over the weaker relation between Pre FC estimate and GS norm and the average Post FC estimates become significantly anti-correlated with the GS norm ($r = -0.72, p < 10^{-3}$).

The average Pre FC estimates in Zone II in Fig. 8b are significantly greater than those in Zone I in panel (a) ($p < 10^{-3}$, paired two-tailed *t*-test). This means that BOLD signals residing in Zone II exhibit greater intrinsic similarity (on average) to the seed signal as compared to those in Zone I. To verify this, in Fig. 11a we plot the correlations between the seed signal (PCC) and the average BOLD signal in Zone II versus the correlations between the seed signal and the average BOLD signal in Zone I. The average BOLD signal in Zone II was significantly ($p < 10^{-3}$, paired two-tailed *t*-test) more correlated with the seed signal compared to Zone I.

In Fig. 11b we plot the correlations between the GS and the average BOLD signal in Zone II versus the correlations between the GS time course and the average BOLD signal in Zone I. We found no significant difference ($p = 0.45$, paired two-tailed *t*-test) between those correlation values for Zone I and Zone II. This means that the GS regressor exhibits a similar range of correlations to the raw time courses in both zones. This is consistent with the fact that the average ΔFC values in the two zones (black squares in Fig. 9) were highly correlated across scans with each other ($r = 0.94$). In addition, the relation between the per-voxel ΔFC values and the orthogonal nuisance fractions were similar in the two zones as shown by the linear fits in Fig. 10 with $r = 0.93$ for Zone I and $r = 0.89$ for Zone II.

In summary, the difference in Zone I and Zone II behavior reflects two effects. First, GSR results in a similar range of ΔFC values for both zones as shown in Fig. 10a and b. This was largely because the GS time courses were similarly related to the average BOLD signals in Zone I and Zone II (Fig. 11b) and thus the orthogonal nuisance fraction fractions between the GS and seed-voxel pairs in the two zones were similar, as shown in Fig. 10. Second, FC estimates in Zone II were significantly greater as compared to those in Zone I and exhibited a weaker dependency on the GS norm (slope 0.041, $r = 0.69$) in Fig. 9b as compared to Zone I (slope 0.11, $r = 0.87$).

Fig. 11a shows that brain regions that are intrinsically similar to the seed signal are more likely to belong to Zone II. The specific brain regions that exhibit either Zone I limitation (residual positive correlation between the GS norm and Post FC estimates) or Zone II limitation (an introduced negative correlation between the GS norm and Post FC estimates) vary with the seed signal used. These regions can be determined by looking at the GS contamination maps after GSR for other seeds as provided in the Supplementary Figs. 11–14. Table 1 summarizes the relation between the GS norm and FC estimates.

As a supplementary experiment, we performed multiple HM+WM+CSF+GS regression. We provide the nuisance contamination maps and correlations in Supplementary Fig. 15 using the PCC seed. The contamination maps, correlation distributions, and significance results in Table 1 for the multiple regression were very similar to those obtained with GSR.

3.4. Between-subject and within-subject effects

To characterize the contributions of between-subject and within-subject variations on the relation between nuisance norms and FC estimates, we conducted an additional analysis in which the correlations were computed when (1) using the subject mean FC estimates and nuisance norms and 2) regressing out the individual subject means from the FC estimates and nuisance norm values. For each of these two conditions and each of the 5 different seed regions considered in Table 1, we computed the number of significant correlations observed between the resultant FC estimates and nuisance norms, both before and after nuisance regression. We also computed the mean and standard deviation of the percent variance explained in these conditions across the significant seed-voxel pairs. In order to simplify the presentation, the results were averaged over the 5 different seed regions.

As a baseline, the first partition in Table 2 shows the results from Table 1 averaged across the 5 seed types. The second partition presents the results obtained when considering the subject mean metrics, while the third partition displays the results obtained when the subject means are regressed out of the metrics. As compared to the baseline results, the subject mean results have a smaller number of significant correlations, but the nuisance norms explain a considerable percent of the variance in the FC estimates for the correlations that are significant. For results obtained after regressing out subject means, the number of significant

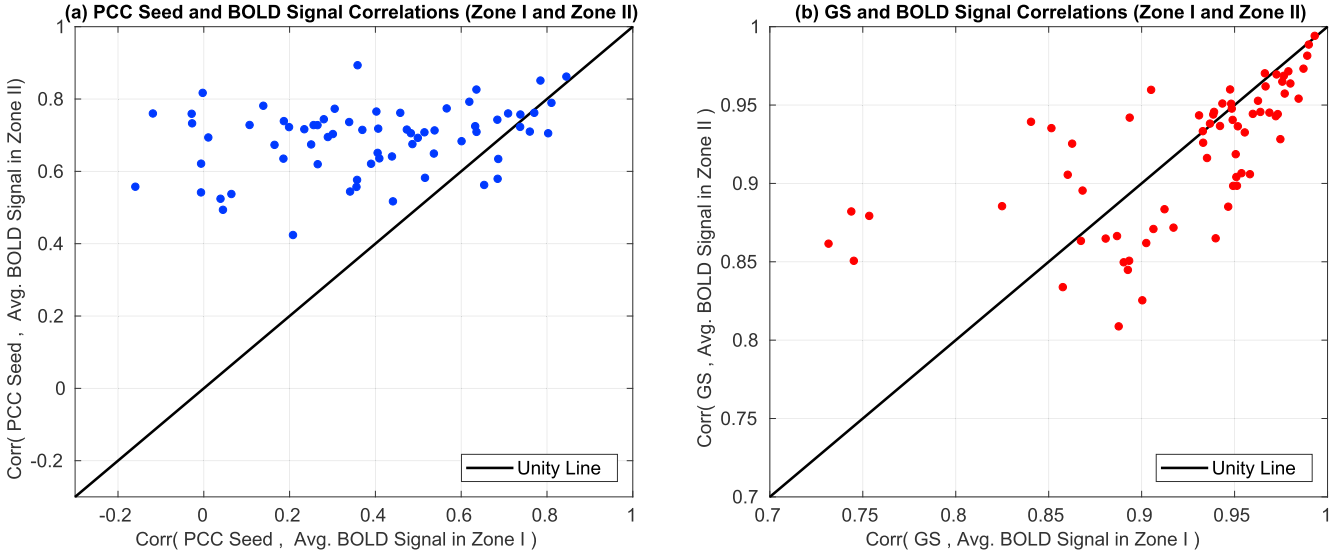

Fig. 11. In (a) we show the correlations obtained between the PCC seed and the average BOLD signal in Zone II versus the correlations obtained between the PCC seed and the average BOLD signal in Zone I. The average BOLD signal in Zone II was significantly ($p < 10^{-3}$, paired two-tailed *t*-test) more correlated with the PCC seed signal as compared to Zone I. This means that brain regions that are more similar to the seed signal are more likely to have the Zone II limitation of GSR. In (b) we show the correlations between the GS and the average BOLD signal in Zone II versus the correlations between the GS and the average BOLD signal in Zone I. We found no significant difference ($p = 0.45$, paired two-tailed *t*-test) between Zone I and Zone II correlations. This indicates that on average, the differences in Zone I and Zone II effects are not dependent on the relation between the GS and the underlying BOLD time courses in those zones.

Table 2
Between-subject and within-subject contributions to the relationship between FC estimates and nuisance norms. 1) Baseline values obtained by averaging results from Table 1 across all seed types. 2) Percentage of seed-voxel pairs with significant correlations and percent variance explained between the FC estimates and nuisance norms when using the subject mean values. 3) Percentage of seed-voxel pairs with significant correlations and percent variance explained when regressing out the subject mean values from FC estimates and nuisance norms.

	State	HM		HM+WM+CSF		GS		HM+WM+CSF+GS	
		%Brain	%Var mean±SD	%Brain	%Var mean±SD	%Brain	%Var mean±SD	%Brain	%Var mean±SD
1. Overall Correlations	Pre FC	47	12±4	96	28±10	98	41±13	97	32±11
	Post FC	51	12±4	70	15±7	25	12±5	23	11±5
2. Subject Means Only	Pre FC	21	31±6	75	41±11	87	51±14	81	44±12
	Post FC	21	32±6	32	34±9	10	32±8	9	32±8
3. Subject Means Regressed	Pre FC	10	8±2	84	17±7	99	29±10	92	20±9
	Post FC	16	9±2	25	10±3	10	9±3	12	9±3

correlations is comparable to the subject mean results, but the percent variance explained is smaller. Overall, these results indicate that while nuisance norms can explain a portion of both the within-subject and between-subject variance in FC estimates, they can explain a greater portion of the between-subject variance.

4. Discussion

We have shown that inter-scan variations in FC estimates can be strongly and significantly correlated with the geometric norms of various nuisance measurements. We found that the relationship between the FC estimates and nuisance norms can persist even after performing multiple nuisance regression. We used the mathematical framework developed in (Nalci et al., 2019) to describe the limitations of nuisance regression with regards to static FC measures and demonstrated that the empirical results were in agreement with the theoretically predicted bounds.

For non-GS regressors (i.e. HM and HM+WM+CSF), we found nuisance regression to be largely ineffective. This was because non-GS regressors were largely orthogonal to the measured BOLD data, as shown in Fig. 5, with mean orthogonal nuisance fractions ranging from 0.70 to 0.99. The large orthogonality imposed tight bounds on the difference between the FC estimates obtained before and after nuisance regression, which in turn limited the ability of regression to reduce the strength of the correlation between the nuisance norms and the FC estimates. This limitation for non-GS regression applied to static FC measures is largely consistent with our previous findings for dynamic FC measures (Nalci et al., 2019).

We introduced *nuisance contamination maps* to visualize the effects of nuisance norms on the FC estimates both before and after nuisance regression. These maps serve as a useful tool in analyzing the spatial location and extent of nuisance contamination present in seed-based FC estimates across scans. In Figs. 3 and 6, the FC estimates obtained between the PCC seed and BOLD signals from other brain regions exhibited strong correlations with the HM and HM+WM+CSF norms both before and after nuisance regression. As summarized in Table 1, depending on the seed signal, 40–100% of the seed-voxel pairs in the brain exhibited significant correlations with respective nuisance norms prior to nuisance regression. After nuisance regression, FC estimates from 43% to 82% of the seed-voxel pairs still exhibited significant correlations with nuisance norms. This means that FC estimates are highly correlated with different nuisance norms even after nuisance regression. The presence of these significant correlations indicates that differences in FC estimates will partly reflect variations in the strengths of nuisance effects, thereby complicating the interpretation of studies that aim to compare FC estimates across subjects, groups, and conditions.

4.1. GSR specific findings

We found that GSR removed a large portion of the GS norm fluctuations from the FC estimates across scans. However, depending on the seed signal, a considerable portion (20–30%) of the FC estimates still remained significantly correlated with the GS norm. In addition, GSR introduced a negative correlation between the FC estimates and GS norm in some voxels.

To better understand the behavior of GSR, we divided the brain into two spatially non-overlapping regions, corresponding to Zones I and II. The changes in FC (ΔFC) caused by GSR showed a similar negative dependence on the GS norm in both zones. Although the Pre FC values in both zones showed a positive dependence on the GS norm, the slope was smaller for the Zone II voxels, reflecting a weaker dependence. Due to this difference in slopes, significant negative correlations between the GS norm and inter-scan FC estimates were observed after GSR in Zone II, whereas the GS norm remained significantly positively correlated with inter-scan FC estimates in Zone I.

The GS contamination maps obtained with the PCC seed in Fig. 7b resembled PCC-based FC maps obtained after GSR (Fox et al., 2005; Murphy and Fox, 2017). It is known that GSR increases the spatial extent and strength of anti-correlations present in resting-state FC maps, especially between the default-mode (DMN) and task-positive networks (TPN) (Fox et al., 2005, 2009; Saad et al., 2012; Murphy et al., 2009; Murphy and Fox, 2017). Indeed a great deal of the controversy concerning the use of GSR has centered on whether the observed anti-correlations are real or artifactual (Murphy and Fox, 2017; Nalci et al., 2017). Despite the visual similarity of the two types of maps, it is important to stress that they depict two fundamentally different quantities, with the contamination maps showing the relation between the GS norm and FC estimates across scans.

To better understand the similarity in the appearance of the two types of maps, we first note that the weaker dependence of the Zone II Pre FC values on the GS norm was associated with the presence of significantly higher Pre FC values in this zone as compared to Zone I. This association suggests that the FC measures for voxels that are more strongly correlated with the seed signal exhibit a weaker sensitivity to variations in the norm of the GS as compared to voxels with a weaker correlation. For the PCC seed, the TPN region resided in Zone I and the DMN region resided in Zone II, consistent with a stronger correlation with the PCC for voxels in the DMN. In both zones, GSR produced a similarly sized negative offset (mean of −0.37) on the Pre FC estimates. The observation of a negative offset is consistent with prior findings (Murphy et al., 2009). As a result of this negative offset and the underlying differences in the Pre FC values, the mean FC estimates in Zone I in Fig. 9a became negative after GSR, while the FC estimates in Fig. 9b remained largely positive. To summarize, Zone I voxels exhibit both a positive dependence on GS norm and negative FC values after GSR, whereas Zone II voxels exhibit both a negative dependence on GS norm and positive FC values after GSR. These associations give rise to the similarity in the maps.

The current findings add additional factors to consider in the ongoing controversy regarding the use of GSR (Murphy and Fox, 2017; Nalci et al., 2017; Liu et al., 2017; Glasser et al., 2018). Prior to GSR a high percentage (>96%) of the FC estimates were significantly correlated with the GS norm, with the GS norm accounting for 40 ± 12 percent of the variance in the whole-brain FC estimates across scans and different seeds.

This means that differences in GS norms can largely drive variations in FC metrics across scans when GSR is not performed. As discussed below, this dependence may partly reflect variations in vigilance across scans. On the other hand, when GSR is performed, the strength of the relation between the FC estimates and the GS norms is reduced, but there is a risk of introducing negative correlations between the GS norm and inter-scan FC estimates. Further work is needed to assess the impact of these negative correlations on the interpretation of FC studies.

4.2. Studies investigating FC across scans

A multitude of fMRI studies have investigated the differences in FC measures between disease populations and healthy controls. Examples of such studies include investigations of Alzheimer's disease (Greicius et al., 2004; Yang et al., 2014; Wang et al., 2007), Parkinson's disease (Baudrexel et al., 2011), depression (Greicius et al., 2007), schizoprenia (Liu et al., 2008), dementia (Rombouts et al., 2009), and amyotrophic lateral sclerosis (ALS) (Mohammadi et al., 2009; Agosta et al., 2013). While these studies all used some type of nuisance regression to remove the potential effects of nuisance terms on their analyses, our results strongly indicate that the results may still have exhibited a relation between the FC estimates and the nuisance norms.

As an example, in (Baudrexel et al., 2011) the authors observed an increased subthalamic nucleus-motor cortex FC in Parkinson's disease as compared to healthy controls. They compared HM measures across the Parkinson's and healthy control groups but did not find a significant difference. However, they did not directly consider either the relation between HM measures and FC estimates or potential group differences in the variation of HM parameters across each group. We have shown that HM norms can be strongly correlated with the FC estimates across scans both before and after regression. Based on our findings, it is possible that inter-group differences in the variability of HM measures could have affected the finding of FC differences. We believe that any future study that compares FC estimates across subject groups should also consider the potential link between FC estimates and nuisance norms.

4.3. Limitations of linear regression

fMRI studies typically rely on linear regression to remove nuisance effects from BOLD data by either using direct nuisance measurements (Bright et al., 2017; Power et al., 2012, 2015; Glover et al., 2000; Chang et al., 2009; Chang and Glover, 2009) or using a set of nuisance regressors derived with data-driven methods (Behzadi et al., 2007; Pruim et al., 2015; Glasser et al., 2018). The performance of these methods is usually characterized by their effects on raw BOLD signals on a per-scan basis (e.g. the percentage of variance removed). The ability of these techniques to reduce the relation between FC estimates and nuisance norms has not been as fully explored (Nalci et al., 2019). As shown in both (Nalci et al., 2019) and the present work, the ability of linear regression methods to reduce the strength of the relation between FC estimates and nuisance norms can be quite limited even when the regressor exhibits only a moderate degree of orthogonality to the BOLD data. This limitation holds regardless of whether a regressor is obtained using data-driven methods or measured directly. Further work is needed to develop nuisance mitigation methods that can go beyond the limitations of linear regression approaches.

4.4. Nuisance norm regression

The present study shows the limited efficacy of nuisance regression in reducing the relation between nuisance norms and FC estimates across scans. Given this limitation, a reasonable approach is to perform nuisance norm regression (NNR) on the inter-scan FC estimates. This approach was originally proposed in Nalci et al. (2019) for cleaning sliding-window dynamic FC estimates and involves projecting out the nuisance norms from inter-scan FC estimates. Though this method would ensure orthogonality between the nuisance norms and inter-scan FC estimates, it might not be a suitable approach for cleaning static FC estimates.

One potential issue with NNR for static FC estimates is the presence of leverage effects (Hoaglin and Welsch, 1978; Draper and Smith, 2014). In computing the regression fit coefficient between the nuisance norms and inter-scan FC estimates, scans with larger nuisance norms will have greater leverage on the regression equation. This means that a scan with a large nuisance norm value can have a relatively greater influence on the fit coefficient. Therefore, although NNR can eliminate the correlation between FC estimates and nuisance norms across scans, there may be potential issues that require further study. Future work and new approaches are of interest to understand how to best minimize nuisance norm effects in inter-scan FC estimates.

4.5. Vigilance effects

There is growing evidence that changes in vigilance are responsible for a considerable portion of the resting-state fMRI signal (Wong et al., 2012, 2013; 2015; Liu et al., 2017; Falahpour et al., 2018). Vigilance fluctuations can account for approximately 10–20% of the variance in the whole-brain GS, while differences in mean vigilance levels can account for 25% of the variance in the GS norm across a sample and 64–81% of the differences in GS norms observed between conditions (Liu et al., 2017). In addition, Falahpour et al. (2018) demonstrated large variations in the vigilance norm (i.e. standard deviation of vigilance fluctuations within a scan) across scans. Our results in Table 1 reveal that inter-scan FC estimates are strongly related to fluctuations in the GS norm across scans. Given the reported relations between the GS and vigilance measures, it is likely that variations in static FC estimates will exhibit a dependence on variations in vigilance. The information contained in the GS norm and the static FC estimates may therefore prove to be useful for assessing inter-subject and inter-scan variations in arousal and vigilance. Further work to study the relation between GS and vigilance norms and FC estimates will be helpful.

4.6. Nuisance norm considerations and scan quality

In this work we used the nuisance (Euclidean) norm to measure the relative strength of various nuisance terms across the whole scan duration. In some cases, the nuisance norm will be related to the overall scan quality. For example, when there are elevated levels of motion, a higher motion-related nuisance norm will tend to reflect the lower quality of a scan. However, it is important to stress that both the norm and scan quality will depend on the types of processing that have been applied to the data. In the case of motion, a scan may have a high motion nuisance norm (and thus low scan quality) prior to motion censoring but have a much lower norm (and thus higher scan quality) after motion censoring. For other cases, there may not be a direct relation between the nuisance norm and scan quality. For example, the global signal norm may be very high in a subject with low trait vigilance, but the scan may still be assessed to have high quality since the data reflect the physiological state of the subject. Finally, it is important to note that while a nuisance norm may sometimes be a reflection of scan quality, its primary purpose is to characterize the strength of the associated nuisance term. For a given study, it remains to the investigator to determine how best to interpret correlations that are observed between the nuisance norm and static FC estimates.

For multiple regressors, the nuisance norm was calculated as the square root of the sum over all regressors of the respective squared norms (see Section 2.4). As different types of regressors have different intrinsic units (e.g. *mm* for motion and percent change (%Δ) for BOLD signals), the nuisance norm for multiple regressors will depend on the relative weighting of the norms for different regressor types. Because the expected numerical values of the different regressor types used in this work are roughly of the same order (i.e. ~1 *mm* for motion or ~1% for BOLD signal change), the flat weighting across regressor types (as stated in

Section 2.4) represents a reasonable choice. This is supported by the observation that the ranges spanned by the various regressor norms in the example data of Figs. 2, 3 and 7 are roughly of the same order. However, it is possible that other weightings of the different regressor types might elucidate a stronger connection between nuisance norms and FC estimates, and a future investigation of alternate weighting schemes may be useful. Note that we did not normalize the time courses to be *unit norm* for each regressor type as this would eliminate the fluctuations of the nuisance norms across different scans (i.e. norms would be constant across scans). An alternative approach would be to use a general linear model to consider the relation between the FC estimates and multiple nuisance norms.

4.7. Nuisance regressors

The nuisance regressors used in this paper represent standard regressors that are widely used in the field (Murphy et al., 2013; Liu, 2016; Liu et al., 2017). A potential limitation is that they are derived from the fMRI data and may therefore not be truly independent of the FC values. However, given their widespread use and the current view that these data-driven regressors partly represent nuisance effects, it is nonetheless of interest to understand the relation between the regressor norms and FC estimates both before and after nuisance regression. The framework work presented here is readily extended to any nuisance regressor, and further work to examine the relation between static FC estimates and the norms of other types of regressors, such as independently acquired measures of physiology, would be of interest.

For the calculation of WM and CSF regressors, we adopted the approach described in our prior work (He and Liu, 2012; Nalci et al., 2017), which used spherical ROIs situated in deep white matter and the lateral ventricles. A similar approach using small seed regions in ventricular and white matter regions was described in the influential studies of (Fox et al., 2005, 2009). Another common approach is to use segmentation of anatomical data to define subject-specific WM and CSF partial volume maps. After thresholding and erosion of the maps, regressors can be defined using either the mean or principal components of the signals from the WM and CSF regions (Behzadi et al., 2007; Whitfield-Gabrieli and Nieto-Castanon, 2012). The size of the defined regions will depend on the specific thresholding and erosion parameters, which can vary widely across studies. For example, Behzadi et al. (2007) recommended using a threshold of 0.99 with two voxels of erosion, whereas the default parameters in the widely used Conn toolbox (Whitfield-Gabrieli and Nieto-Castanon, 2012) specify a threshold of 0.50 with one voxel of erosion. Higher thresholds and more aggressive erosion result in smaller regions, similar in size to the small WM and CSF seed regions used in this and prior work. On the other hand, lower thresholds and less aggressive erosion leads to larger regions and an increased probability that the WM and CSF signals may contain gray matter signals and therefore become more similar to the global signal. This is partly reflected in the fact that regression using WM and CSF signals defined with the Conn parameters results in FC maps that are more similar to those obtained with GSR as compared with FC maps obtained with smaller seed regions (Chai et al., 2012; Fox et al., 2009). These results are roughly consistent with our finding that global signal regression had a much greater effect on the nuisance norm contamination maps as compared with regression using only the HM+WM+CSF regressors. Based on the prior work, we anticipate that the use of larger WM and CSF regions would lead to results more similar to those obtained with global signal regression and acknowledge that future work to assess the effects may be useful.

5. Conclusion

We have provided a detailed examination of nuisance effects and the efficacy of nuisance regression on the variability of FC estimates across scans. We have shown that the norms of various nuisance terms can be strongly and significantly correlated with variations in inter-scan FC estimates both before and after nuisance regression. We found that non-GS regressions (HM, HM+WM+CSF) were largely ineffective in reducing the correlations between nuisance norms and FC estimates. We showed that though GSR removed a large fraction of the GS norm fluctuations from the FC estimates, a considerable portion ($20-30\%$) of the FC estimates still remained significantly correlated with the GS norm. In addition, significant negative correlations between the GS norm and FC estimates were introduced by the process.

This work stresses an important issue in the interpretation of FC measures. Most FC studies implicitly assume that the effects of nuisance terms on FC estimates are minimized by nuisance regression in the preprocessing stage. Our findings strongly suggest that the interpretation of FC measures should also consider correlations with the nuisance norms that can persist even after nuisance regression. If the relationship between FC estimates and nuisance norms is not considered, differences in FC estimates may be incorrectly interpreted as meaningful effects, when in fact they may be largely due to differences in nuisance activity. This is especially true in studies comparing FC measures between disease groups or treatment conditions.

As we have shown, linear regression-based nuisance removal approaches exhibit theoretical limitations with regards to their ability to reduce the correlations between FC estimates and nuisance norms. Future FC studies will greatly benefit from the development of nuisance removal approaches that can address the limitations highlighted in this work.

Acknowledgments

This work was partially supported by NIH grant R21MH112155 and a UC San Diego Frontiers of Innovation Scholars Program (FISP) Project Fellowship.

Appendix A. Supplementary data

Supplementary data to this article can be found online at https://doi.org/10.1016/j.neuroimage.2019.07.018.

References

Agosta, F., Canu, E., Valsasina, P., Riva, N., Prelle, A., Comi, G., Filippi, M., 2013. Divergent brain network connectivity in amyotrophic lateral sclerosis. Neurobiol. Aging 34 (2), 419–427.

Baudrexel, S., Witte, T., Seifried, C., von Wegner, F., Beissner, F., Klein, J.C., Steinmetz, H., Deichmann, R., Roeper, J., Hilker, R., 2011. Resting state fMRI reveals increased subthalamic nucleus–motor cortex connectivity in Parkinson's disease. Neuroimage 55 (4), 1728–1738.

Behzadi, Y., Restom, K., Liau, J., Liu, T.T., Aug 2007. A component based noise correction method (CompCor) for BOLD and perfusion based fMRI. Neuroimage 37 (1), 90–101.

Birn, R.M., Smith, M.A., Jones, T.B., Bandettini, P.A., Apr. 2008. The respiration response function: the temporal dynamics of fMRI signal fluctuations related to changes in respiration. Neuroimage 40 (2), 644–654.

Biswal, B., Yetkin, F.Z., Haughton, V.M., Hyde, J.S., Oct. 1995. Functional connectivity in the motor cortex of resting human brain using echo-planar MRI. Magn. Reson. Med. 34 (4), 537–541.

Bright, M.G., Murphy, K., Jul. 2015. Is fMRI "noise" really noise? Resting state nuisance regressors remove variance with network structure. Neuroimage 114, 158–169.

Bright, M.G., Tench, C.R., Murphy, K., 2017. Potential pitfalls when denoising resting state fmri data using nuisance regression. Neuroimage 154, 159–168.

Chai, X.J., Castañón, A.N., Ongür, D., Whitfield-Gabrieli, S., Jan. 2012. Anticorrelations in resting state networks without global signal regression. Neuroimage 59 (2), 1420–1428.

Chang, C., Cunningham, J.P., Glover, G.H., Feb. 2009. Influence of heart rate on the BOLD signal: the cardiac response function. Neuroimage 44 (3), 857–869.

Chang, C., Glover, G.H., Oct. 2009. Effects of model-based physiological noise correction on default mode network anti-correlations and correlations. Neuroimage 47 (4), 1448–1459.

Cox, R.W., Jun 1996. AFNI: software for analysis and visualization of functional agnetic resonance neuroimages. Comput. Biomed. Res. 29 (3), 162–173.

Draper, N.R., Smith, H., Aug. 2014. Applied Regression Analysis, third ed. John Wiley & Sons.

Falahpour, M., Nalci, A., Liu, T.T., 2018. The effects of global signal regression on estimates of resting-state blood oxygen-level-dependent functional magnetic

resonance imaging and electroencephalogram vigilance correlations. Brain Connect. 8 (10), 618–627.
Fox, M.D., Raichle, M.E., Sep. 2007. Spontaneous fluctuations in brain activity observed with functional magnetic resonance imaging. Nat. Rev. Neurosci. 8 (9), 700–711.
Fox, M.D., Snyder, A.Z., Vincent, J.L., Corbetta, M., Van Essen, D.C., Raichle, M.E., 2005. The human brain is intrinsically organized into dynamic, anticorrelated functional networks. Proc. Natl. Acad. Sci. 102 (27), 9673–9678.
Fox, M.D., Snyder, A.Z., Vincent, J.L., Raichle, M.E., 2007. Intrinsic fluctuations within cortical systems account for intertrial variability in human behavior. Neuron 56 (1), 171–184.
Fox, M.D., Zhang, D., Snyder, A.Z., Raichle, M.E., Jun. 2009. The global signal and observed anticorrelated resting state brain networks. J. Neurophysiol. 101 (6), 3270–3283.
Glasser, M.F., Coalson, T.S., Bijsterbosch, J.D., Harrison, S.J., Harms, M.P., Anticevic, A., Essen, D.C.V., Smith, S.M., 2018. Using temporal ICA to selectively remove global noise while preserving global signal in functional MRI data. Neuroimage 181, 692–717.
Glover, G.H., Li, T.Q., Ress, D., Jul. 2000. Image-based method for retrospective correction of physiological motion effects in fMRI: RETROICOR. Magn. Reson. Med. 44 (1), 162–167.
Greicius, M.D., Flores, B.H., Menon, V., Glover, G.H., Solvason, H.B., Kenna, H., Reiss, A.L., Schatzberg, A.F., 2007. Resting-state functional connectivity in major depression: abnormally increased contributions from subgenual cingulate cortex and thalamus. Biol. Psychiatry 62 (5), 429–437.
Greicius, M.D., Srivastava, G., Reiss, A.L., Menon, V., 2004. Default-mode network activity distinguishes Alzheimer's disease from healthy aging: evidence from functional MRI. Proc. Natl. Acad. Sci. 101 (13), 4637–4642.
Hallquist, M.N., Hwang, K., Luna, B., Nov. 2013. The nuisance of nuisance regression: spectral misspecification in a common approach to resting-state fMRI preprocessing reintroduces noise and obscures functional connectivity. Neuroimage 82, 208–225.
He, H., Liu, T.T., Feb 2012. A geometric view of global signal confounds in resting-state functional MRI. Neuroimage 59 (3), 2339–2348.
Hoaglin, D.C., Welsch, R.E., Feb. 1978. The hat matrix in regression and ANOVA. Am. Statistician 32 (1), 17–22.
Hutchison, R.M., Womelsdorf, T., Allen, E.A., Bandettini, P.A., Calhoun, V.D., Corbetta, M., Della Penna, S., Duyn, J.H., Glover, G.H., Gonzalez-Castillo, J., Handwerker, D.A., Keilholz, S., Kiviniemi, V., Leopold, D.A., de Pasquale, F., Sporns, O., Walter, M., Chang, C., Oct. 2013. Dynamic functional connectivity: promise, issues, and interpretations. Neuroimage 80, 360–378.
Lacadie, C.M., Fulbright, R.K., Rajeevan, N., Constable, R.T., Papademetris, X., 2008. More accurate Talairach coordinates for neuroimaging using non-linear registration. Neuroimage 42 (2), 717–725.
Liu, T.T., Sep. 2016. Noise contributions to the fMRI signal: an overview. Neuroimage 143, 141–151.
Liu, T.T., Nalci, A., Falahpour, M., 2017. The global signal in fMRI: nuisance or Information? Neuroimage 150, 213–229.
Liu, Y., Liang, M., Zhou, Y., He, Y., Hao, Y., Song, M., Yu, C., Liu, H., Liu, Z., Jiang, T., 2008. Disrupted small-world networks in schizophrenia. Brain 131 (4), 945–961.
Mohammadi, B., Kollewe, K., Samii, A., Krampfl, K., Dengler, R., Münte, T.F., 2009. Changes of resting state brain networks in amyotrophic lateral sclerosis. Exp. Neurol. 217 (1), 147–153.
Murphy, K., Birn, R.M., Bandettini, P.A., 2013. Resting-state fMRI confounds and cleanup. Neuroimage 80, 349–359.
Murphy, K., Birn, R.M., Handwerker, D.A., Jones, T.B., Bandettini, P.A., Feb. 2009. The impact of global signal regression on resting state correlations: are anti-correlated networks introduced? Neuroimage 44 (3), 893–905.
Murphy, K., Fox, M.D., Nov. 2017. Towards a consensus regarding global signal regression for resting state functional connectivity MRI. Neuroimage 154, 169–173.
Nalci, A., Rao, B.D., Liu, T.T., 2017. Global signal regression acts as a temporal downweighting process in resting-state fMRI. Neuroimage 152, 602–618.
Nalci, A., Rao, B.D., Liu, T.T., 2019. Nuisance effects and the limitations of nuisance regression in dynamic functional connectivity fMRI. Neuroimage 184, 1005–1031.
Power, J.D., Barnes, K.A., Snyder, A.Z., Schlaggar, B.L., Petersen, S.E., Feb. 2012. Spurious but systematic correlations in functional connectivity MRI networks arise from subject motion. Neuroimage 59 (3), 2142–2154.
Power, J.D., Schlaggar, B.L., Petersen, S.E., Jan. 2015. Recent progress and outstanding issues in motion correction in resting state fMRI. Neuroimage 105, 536–551.
Preti, M.G., Bolton, T.A., Van De Ville, D., Oct. 2017. The dynamic functional connectome: state-of-the-art and perspectives. Neuroimage 160, 41–54.
Pruim, R.H.R., Mennes, M., van Rooij, D., Llera, A., Buitelaar, J.K., Beckmann, C.F., May 2015. ICA-AROMA: a robust ICA-based strategy for removing motion artifacts from fMRI data. Neuroimage 112, 267–277.
Raichle, M.E., MacLeod, A.M., Snyder, A.Z., Powers, W.J., Gusnard, D.A., Shulman, G.L., 2001. A default mode of brain function. Proc. Natl. Acad. Sci. 98 (2), 676–682.
Rombouts, S.A., Damoiseaux, J.S., Goekoop, R., Barkhof, F., Scheltens, P., Smith, S.M., Beckmann, C.F., 2009. Model-free group analysis shows altered BOLD fMRI networks in dementia. Hum. Brain Mapp. 30 (1), 256–266.
Saad, Z.S., Gotts, S.J., Murphy, K., Chen, G., Jo, H.J., Martin, A., Cox, R.W., 2012. Trouble at rest: how correlation patterns and group differences become distorted after global signal regression. Brain Connect. 2 (1), 25–32.
Satterthwaite, T.D., Wolf, D.H., Loughead, J., Ruparel, K., Elliott, M.A., Hakonarson, H., Gur, R.C., Gur, R.E., Mar 2012. Impact of in-scanner head motion on multiple measures of functional connectivity: relevance for studies of neurodevelopment in youth. Neuroimage 60 (1), 623–632.
Smith, S.M., Miller, K.L., Moeller, S., Xu, J., Auerbach, E.J., Woolrich, M.W., Beckmann, C.F., Jenkinson, M., Andersson, J., Glasser, M.F., Van Essen, D.C., Feinberg, D.A., Yacoub, E.S., Ugurbil, K., Feb. 2012. Temporally-independent functional modes of spontaneous brain activity. Proc. Natl. Acad. Sci. U.S.A. 109 (8), 3131–3136.
Van Den Heuvel, M.P., Pol, H.E.H., 2010. Exploring the brain network: a review on resting-state fMRI functional connectivity. Eur. Neuropsychopharmacol. 20 (8), 519–534.
Van Dijk, K.R., Hedden, T., Venkataraman, A., Evans, K.C., Lazar, S.W., Buckner, R.L., 2010. Intrinsic functional connectivity as a tool for human connectomics: theory, properties, and optimization. J. Neurophysiol. 103 (1), 297–321.
Van Dijk, K.R.A., Sabuncu, M.R., Buckner, R.L., Jan. 2012. The influence of head motion on intrinsic functional connectivity MRI. Neuroimage 59 (1), 431–438.
Wang, K., Liang, M., Wang, L., Tian, L., Zhang, X., Li, K., Jiang, T., 2007. Altered functional connectivity in early Alzheimer's disease: a resting-state fMRI study. Hum. Brain Mapp. 28 (10), 967–978.
Whitfield-Gabrieli, S., Nieto-Castanon, A., 2012. Conn: a functional connectivity toolbox for correlated and anticorrelated brain networks. Brain Connect. 2 (3), 125–141.
Wong, C.W., DeYoung, P.N., Liu, T.T., Aug. 2015. Differences in the resting-state fMRI global signal amplitude between the eyes open and eyes closed states are related to changes in EEG vigilance. Neuroimage 124 (Pt A), 24–31.
Wong, C.W., Olafsson, V., Tal, O., Liu, T.T., Oct. 2012. Anti-correlated networks, global signal regression, and the effects of caffeine in resting-state functional MRI. Neuroimage 63 (1), 356–364.
Wong, C.W., Olafsson, V., Tal, O., Liu, T.T., Dec. 2013. The amplitude of the resting-state fMRI global signal is related to EEG vigilance measures. Neuroimage 83, 983–990.
Yang, G.J., Murray, J.D., Repovs, G., Cole, M.W., Savic, A., Glasser, M.F., Pittenger, C., Krystal, J.H., Wang, X.-J., Pearlson, G.D., Glahn, D.C., Anticevic, A., May 2014. Altered global brain signal in schizophrenia. Proc. Natl. Acad. Sci. U.S.A. 111 (20), 7438–7443.